OBSERVATION OF ISOLATED HIGH-E_T PHOTONS IN PHOTOPRODUCTION AT HERA

by

ANTHONY W. VAICIULIS

A dissertation submitted in partial fulfillment of the requirements for the degree of

Doctor of Philosophy

(Physics)

at the

UNIVERSITY OF WISCONSIN — MADISON

7-30-1998

Abstract

Events containing an isolated prompt photon with high transverse energy, together with a balancing jet, have been observed for the first time in photoproduction at the HERA ep collider at DESY. The data were taken with the ZEUS detector, in a γp center of mass energy range 120-250 GeV. The fraction of the incoming photon energy participating in the production of the prompt photon and the jet, x_γ, shows a strong peak near unity, consistent wit LO QCD Monte Carlo predictions. In the transverse energy and pseudorapidity range $5 \leq E_T^\gamma < 10$ GeV, $-0.7 \leq \eta^\gamma < 0.8$, $E_T^{jet} \geq 5$ GeV, and $-1.5 \leq \eta^{jet} \leq 1.8$ with $x_\gamma^{OBS} > 0.8$, the measured cross section is $15.3 \pm 3.8 \pm 1.8$ pb, in good agreement with a recent NLO calculation.

This is where the acknowledgements go. This is where the acknowledgements go. This is where the acknowledgements go. This is where the acknowledgements go. This is where the acknowledgements go.

Contents

List of Figures

List of Tables

Chapter 1

Introduction

This is the introductory chapter.

1.1 Why are photons interesting?

Why study photons? a (very brief) history.

Chapter 2

Theory

This is the chapter about the theory.

2.1 photoproduction at HERA

ep collisions

Relevant kinematic variables are shown in fig 2.1.

$k = (\vec{k}, iE'_e)$ incident positron four momentum

$p = (0, im_p)$ proton four momentum (in proton rest frame)

$k' = (\vec{k'}, iE'_e)$ scattered positron four momentum

$q = (\vec{k} - \vec{k'}, i\nu)$

$\nu = \frac{p \cdot q}{2m_p} = E_e - E'_e$ (valid in proton rest frame)

$Q^2 = -q^2 = -(k - k')^2$ square of the four momentum transfer

$x = \frac{Q^2}{2p \cdot q}$ fraction of proton momentum carried by the struck parton

$0 \leq x \leq 1$

$y = \frac{p \cdot q}{p \cdot k} = \frac{\nu}{\nu_{max}}$ normalized energy transfer to proton in its rest frame

$\nu_{max} \cong \frac{s}{2m_p} \cong \frac{2E_eE_p}{m_p}$ (E_e = 27.5 GeV and E_p = 821 GeV so HERA is equivalent to a fixed target experiment with an incident lepton beam of 48 TeV)

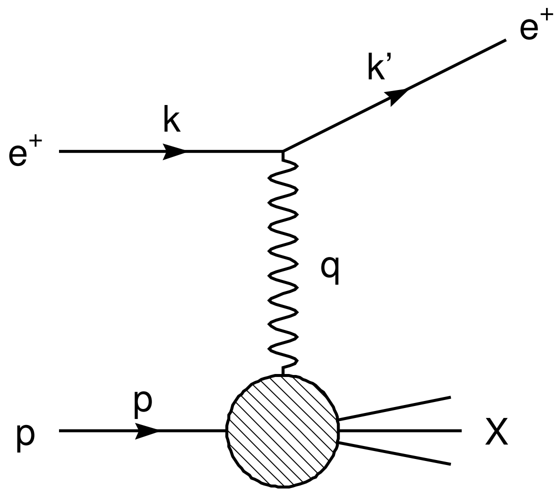

Figure 2.1: definition of kinematic variables for the inelastic scattering process $ep \to eX$

$0 \leq y \leq 1$

$W^2 = (p+q)^2$ square of total mass of final hadronic system X

$s = (p+k)^2 \cong 4E_eE_p$ square of total center of mass energy

Q^2 = sxy

dijet events (diagrams)

DIRECT versus RESOLVED

x_γ=

2.2 the prompt photon process

- diagrams
- theoretical interest
- mention past studies (WA70, UA6, CDF, D0)

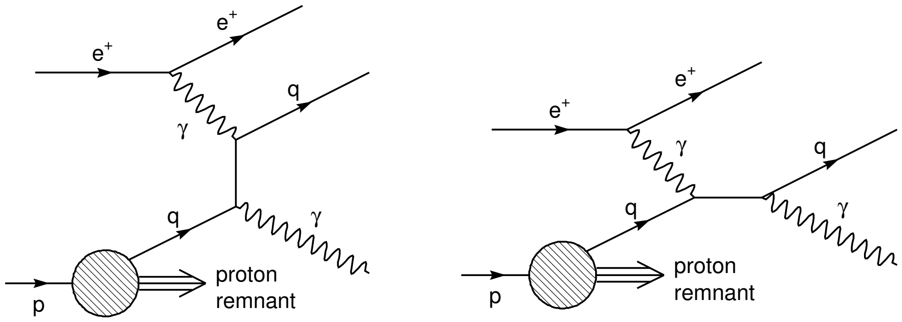

Figure 2.2: direct prompt photon diagrams

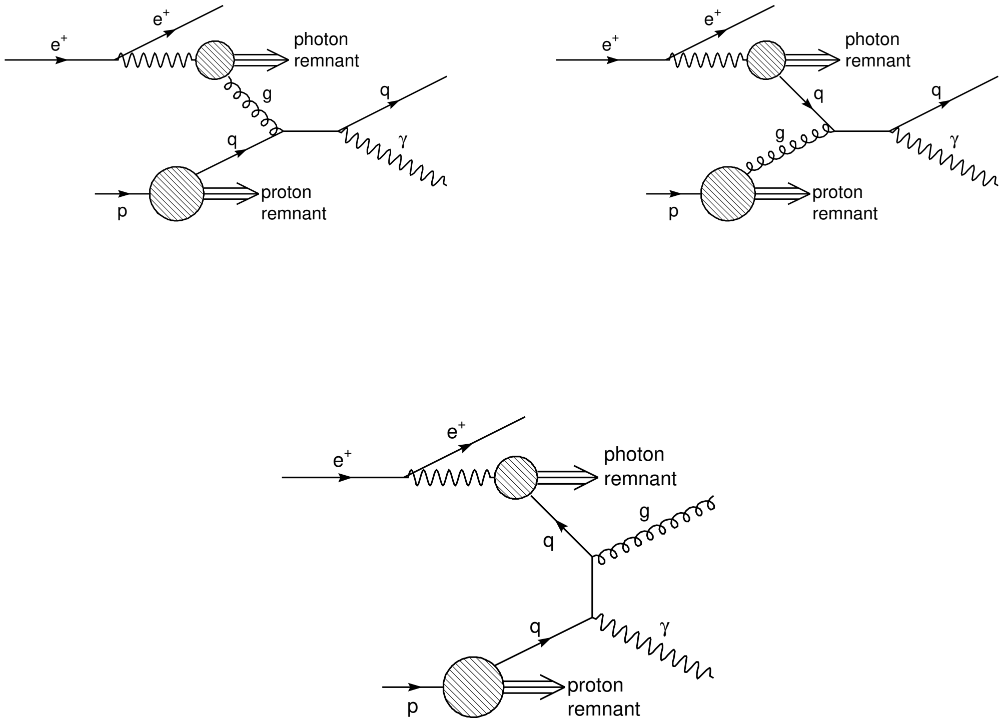

Figure 2.3: resolved prompt photon diagrams

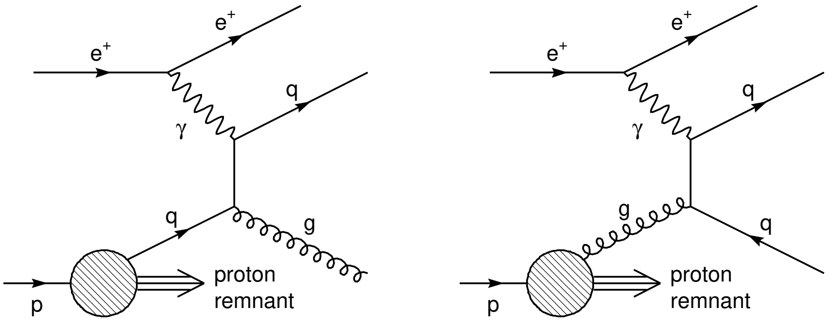

Figure 2.4: direct dijet diagrams

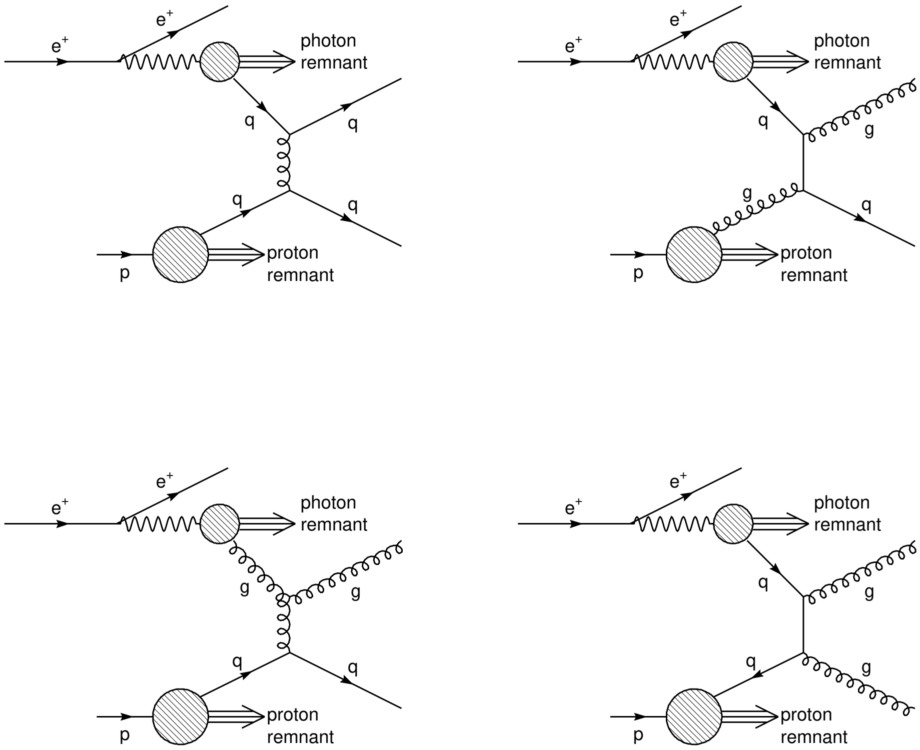

Figure 2.5: resolved dijet diagrams

- What might it tell us at HERA? Recent theoretical papers.

- (mention dijet process is background to prompt photon process here?)

2.3 overview of the analysis

- What questions will be explored in this analysis?

2.4 measurements from other machines

- measurements from other machines

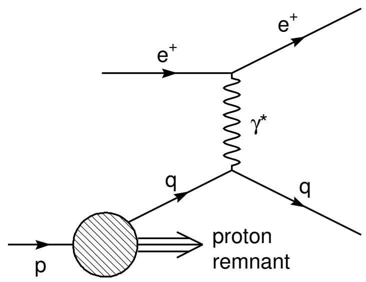

Figure 2.6: an example of the Deep Inelastic Scattering process in which a virtual photon interacts with a quark from the proton.

Chapter 3

Experiment

3.1 The Hadron-Electron Ring Accelerator

The Hadron-Electron Ring Accelerator (HERA) [9], the world's first electron-proton collider, was built at the Deutsches Elektronen-Synchrotron (DESY) Laboratory in Hamburg, Germany to study ep interactions at a much higher Q^2 and a much lower x than previoulsy possible. Q^2 values of 30000 GeV^2 are two orders of magnitude higher than the 230 GeV^2 possible at the fixed target muon experiment BCDMS. This means one can study QCD interactions at distances of a factor of ten smaller than previous experiments. Similarly, values of x as low as 2 x 10^{-5} are two orders of magnitude lower than the values reached at the E665 experiment. Figure 3.1 shows the layout of the HERA facility and table 3.1 lists selected parameters.

Low energy electron/positron or proton beams cannot be stored efficiently in the main HERA ring so a series of preaccelerators is used. Proton injection begins with negative hydrogen ions (H^-) in a 50 MeV Proton Linac. The protons are then accelerated to 7.5 GeV and then to 40 GeV in successive synchrotons before being injected into the HERA proton storage ring where

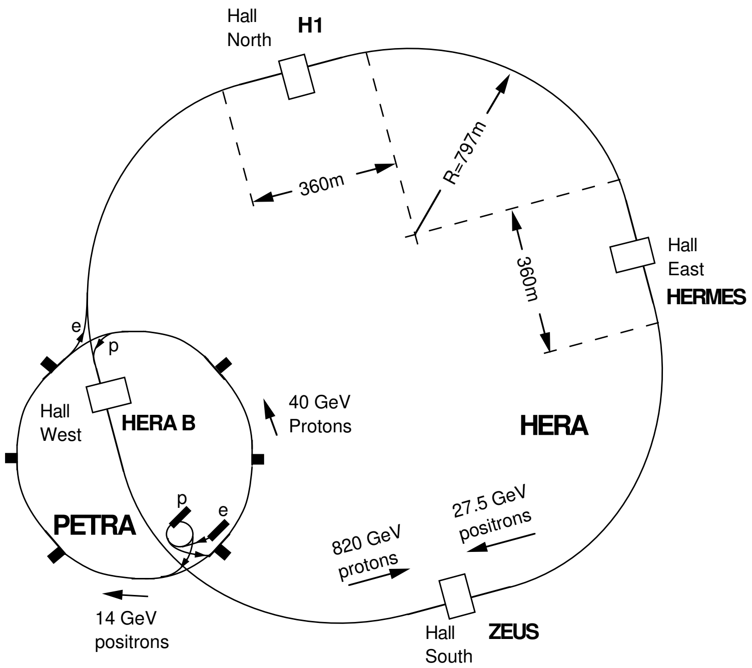

Figure 3.1: View of the HERA facility at DESY.

they reach 821 GeV. The protons are kept in a circular orbit by superconducting dipole magnets which can efficiently achieve the large bending field of 4.7 T. Because of their lower field strength of 1.5 T, normal conducting magnets would require a much larger accelerator ring radius to store 821 GeV protons. The dipoles and focusing quadrupoles are cooled by liquid helium for operation at 4.4 K.

Electrons or positrons are initially accelerated to several hundred MeV in a linear accelerator. In successively more powerful synchrotrons, they attain an energy of 7.5 GeV and then 14 GeV before being injected into the HERA electron storage ring where they reach 27.5 GeV. During data taking in 1995, 27.5 GeV positrons were collided with 821 GeV protons.

construction time	1984 - 1990
physics start date	April 1992
depth underground	10-25 m
inner diameter of tunnel	5.2 m
circumference	6336 m
time between collisions	96 ns

	design values		1995 operation	
	e^-	p	e^+	p
energy (GeV)	30	820	27.5	821
center of mass energy (GeV)	314		300	
instantaneous luminosity ($cm^{-2}s^{-1}$)	1.5 x 10^{31}		(1-6) x 10^{30}	
integrated luminosity (pb^{-1})			12	
particle current (mA)	58	160	10-35	40-70
number of bunches	210	210	174+15	174+6
filling time (min.)	15	20	45	60
beam σ_x (mm) at IP	0.30	0.27	0.27	0.18
beam σ_y (mm) at IP	0.06	0.09	0.06	0.06
beam σ_z (cm) at IP	0.8	0.11	0.8	11
field strength of main dipoles (T)	0.16	4.7		
radiation energy loss per revolution (MeV)	70.38	1.4 x 10^{-10}		

Table 3.1: selected HERA parameters

In both the proton and positron storage rings, the particles are accelerated by radiofrequency (RF) cavities. After the particles reach full energy, the RF cavities serve two main purposes: 1) replace the power lost by the electrons/positrons due to synchrotron radiation and 2) compress the proton bunches longitudinally.

3.2 Interaction of particles with matter

We attempt to learn about the fundamental forces of nature by observing the particles responsible for these forces. Accelerators and detectors are built to study the interactions of these particles with one another. To build these machines and to understand the data they provide, much effort has gone into understanding how particles interact with matter [12,13]. The use of calorimeters to measure the energy of high energy particles is an example of how knowledge of particle interactions with matter is important. There are several distinct kinds of calorimeter energy deposits depending on the type of incident particle. Except for the photon, $W^{\pm}$, Z, and the leptons (e, μ, τ, and ν_e, ν_μ, ν_τ), all other observed particles undergo strong interactions and are called hadrons. This section will briefly describe how hadrons, photons, and leptons behave in matter using their passage through a calorimeter as an example.

Figure 3.2 shows three types of shower development in a calorimeter – a broad, deep hadronic shower, a compact electromagnetic shower, and the energy deposit of a minimum ionizing particle. Hadrons can undergo a large variety of strong interactions with nucleii, resulting in a complicated shower structure. The spatial extent of a hadronic shower is controlled by the nuclear interaction length (absorption length) λ. When a hadron enters a calorimeter, the first interaction will occur, on average, after one nuclear interaction length. The incident hadron produces more hadrons which penetrate more and more deeply into the calorimeter. The shower structure is made more complicated by π°s, which are often produced within a hadronic shower. These decay to two photons creating pure electromagnetic showers within the hadronic shower.

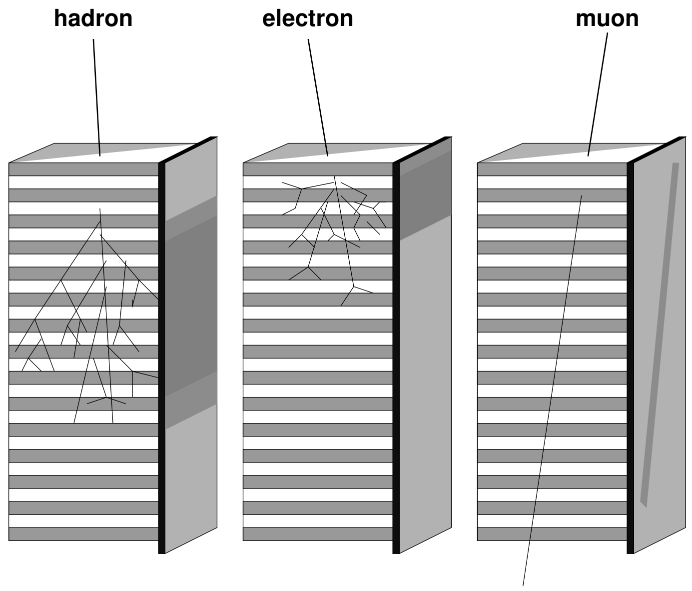

Figure 3.2: Shower development in a calorimeter for a hadron, an electron, and a minimum ionizing particle.

Photons exhibit a behavior in matter which is very different than hadrons. There are three main ways in which energetic photons interact with matter: the photoelectric effect, Compton scattering, and pair production. For low incident photon energies (less than $\sim$1 MeV for lead, less than $\sim$0.01 MeV for carbon) the photoelectric effect is dominant. The total energy of the photon is absorbed by an atomic electron which becomes free. The dominant process at intermediate energies (1-10 MeV for lead, 0.01-100 MeV for carbon) is Compton scattering in which the photon scatters from an atomic electron. The electron normally leaves the atom, carrying a significant fraction of the photon's energy. At high energies the production of electron-positron pairs dominates the photon absorption cross section. To conserve both momentum and energy, the reaction must take place in the presence of a nucleus or atomic electron. Almost all of the photon energy above the threshold of 1.022 MeV is divided between the kinetic energies of the electron and positron since the energy absorbed by recoil of the nucleus or atomic electron is very small.

An important characteristic of photon interactions with matter is the possibility of a catastrophic energy loss. In a single collision, the photon can be completely absorbed by the material. This is in contrast to the gradual energy loss of charged particles.

The different types of leptons (e, μ, τ, and ν_e, ν_μ, ν_τ) behave very differently from each other in matter. Neutrinos have very little interaction with matter and so will pass through a calorimeter leaving no detectable signal. The τ lepton's very short lifetime of about 10^{-13}s means that it decays quickly (to hadrons and other leptons) and does not directly start a calorimeter shower.

Muons and other charged particles lose energy through excitation of atomic electrons and ionization. Unlike charged hadrons, however, muon energy loss is completely dominated by excitation and ionization since muons do not undergo strong interactions. The mean rate of ionization loss for various materials traversed is well understood and given by the Bethe-Bloch formula as the average energy loss per unit path length (dE/dx). In a given material, dE/dx is mainly a function only of $\beta = v/c$. It decreases as $1/\beta^2$ at low (non-relativistic) velocities, reaches a minimum at $\beta \simeq 0.96$, and then increases logarithmically with $\gamma = (1 - \beta^2)^{1/2}$. Particles with $\beta \simeq 0.96$ are called minimum ionizing particles (mip). The actual minimum value of dE/dx is almost the same for all particles of the same charge. Even particles with $\beta >$ 0.96 will behave similarly to a minimum ionizing particle because of the slow rise of dE/dx with respect to energy. Fig 3.2 shows a muon leaving a minimum ionizing signal in a calorimeter. This is a small, constant energy deposit along the path of the particle.

For energies below a few 10's of MeV, electrons and positrons lose energy through excitation of atomic electrons and ionization just as muons and other charged particles do. For energies above a few 10's of MeV, however, the dominant energy loss process for electrons and positrons is bremsstrahlung – the emission of electromagnetic radiation arising from scattering in the electric field of a nucleus. Bremsstrahlung is an important energy loss process only for electrons and positrons because it is inversely proportional to the square of the particle mass. The next lightest charged particle, the muon, has a mass 200 times the electron mass. A quantity frequently used to describe detector material is the radiation length, X_o, defined as the mean distance over which a high energy electron loses all but 1/e of its energy by bremsstrahlung. For a given material, the radiation length is typically many times smaller than the nuclear interaction length (absorption length) λ. Therefore electromagnetic showers (those initiated by electrons, positrons, or photons) are much more compact than hadronic showers.

The middle picture in fig 3.2 is an example of an electromagnetic shower. On average, a high energy electron or positron entering a calorimeter radiates a bremsstrahlung photon after one radiation length. This photon then converts to an electron-positron pair which can then create more photons resulting in a shower of particles. Eventually the individual electrons, positrons, and photons have low enough energy that atomic excitation and ionization are the dominant energy loss mechanisms, rather than bremsstrahlung and pair production. A calorimeter of depth 10 to 25 X_o is typically deep enough to contain most of the energy of an electromagnetic shower. The amount of energy leaking out of the calorimeter depends on the calorimeter depth and the incident particle energy.

3.3 The ZEUS detector

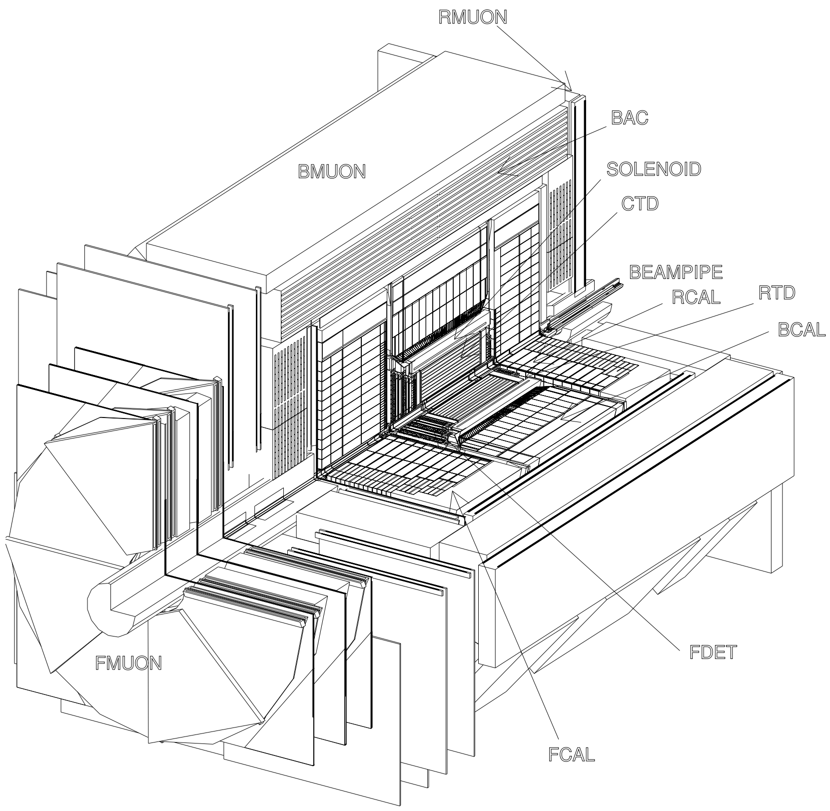

Figure 3.3: Cutaway view of the ZEUS detector.

ZEUS is a multipurpose detector located in the south experimental hall of

HERA. A detailed description can be found in [5]. Only those components most important for the prompt photon analysis will be described here. A cutaway view of the detector in figure 3.3 shows how it surrounds the HERA beampipe. The Central Tracking Detector (CTD) sits in a 1.4 T magnetic field created by a thin superconducting solenoid. Surrounding the solenoid and CTD are the forward, barrel, and rear sections of the uranium calorimeter (FCAL, BCAL, RCAL). The nominal interaction point is at the center of the detector. Protons enter the detector through a hole in the RCAL and move towards the FCAL. This is the +z direction.

The ZEUS coordinate system is shown in figure 3.4. The nominal interaction point (IP) is at (x,y,z) = (0,0,0). The HERA beams move along the z axis (protons in the +z direction, positrons in the -z direction). The azimuthal angle ϕ and the polar angle θ are referred to often in this dissertation and are defined in figure 3.4. The pseudorapidity η is defined as -ln(tan(θ/2)).

3.3.1 Calorimeter

The three sections of the ZEUS calorimeter can be seen in the y-z view in figure 3.5. It covers the angular region $2.5^\circ < \theta < 176.2^\circ$ for all ϕ, which is 99.9% of the solid angle. To accomodate the HERA beam pipe, there is a 20 x 8 cm^2 hole in RCAL and a 20 x 20 cm^2 hole in FCAL. FCAL/BCAL/RCAL covers the angular range $2.5^\circ < \theta < 39.9^\circ$/ $36.7^\circ < \theta < 129.1^\circ$/ $128.1^\circ < \theta < 176.2^\circ$. The ZEUS calorimeter is sampling, with depleted uranium as the absorber and scintillator as the active material. It is fully compensating, with an electron to hadron signal ratio e/h = 1.00 $\pm$ 0.03. This is not a

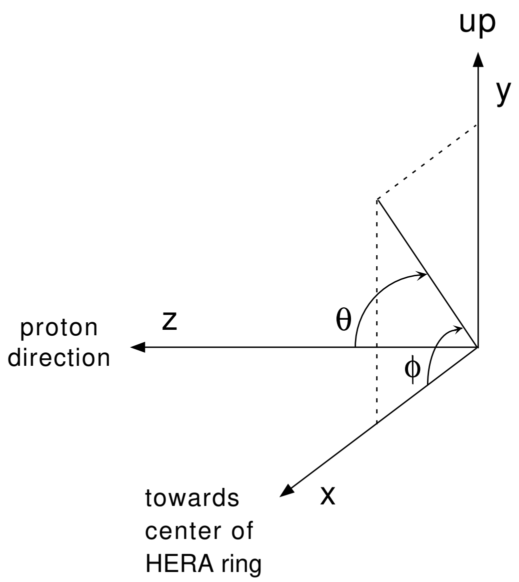

Figure 3.4: The ZEUS coordinate system.

trivial accomplishment since a hadronic particle will typically produce a much smaller signal than an electromagnetic particle of the same energy. Some of the hadron's energy is used for excitation and breakup of absorber nucleii and is not fully observable. From test beam data [14], the energy resolution is $\sigma_{\rm E}/{\rm E} = 0.18/\sqrt{\rm E}$ for electrons/positrons and $\sigma_{\rm E}/{\rm E} = 0.35/\sqrt{\rm E}$ for hadrons (E in GeV). The timing resolution is about 1 ns.

The calorimeter is longitudinally segmented into an electromagnetic section and one (RCAL) or two (FCAL,BCAL) hadronic sections. The electromagnetic sections are about 25 radiation lengths deep to contain most of the energy of an electromagnetic shower. The total depth of the calorimeter ranges from 4 (RCAL) to 7 (FCAL) nuclear interaction lengths, reflecting the very asymmetric HERA beam energies.

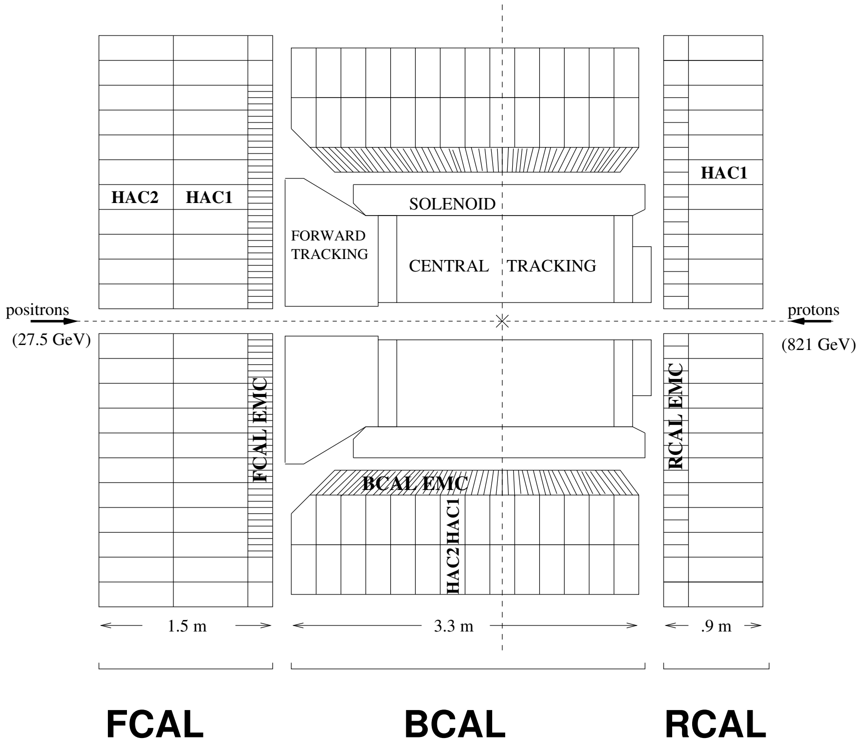

Figure 3.5: y-z projection of the ZEUS calorimeter.

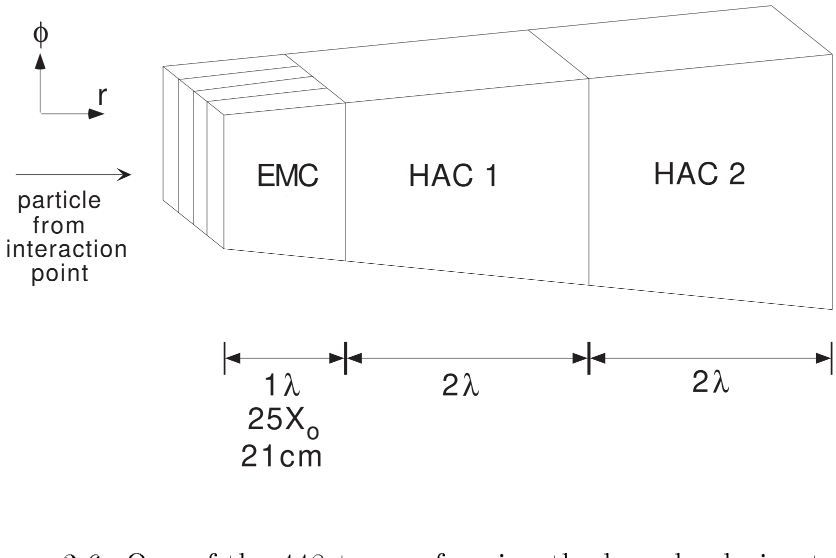

Figure 3.6: One of the 448 towers forming the barrel calorimeter.

The forward (FCAL), barrel (BCAL), and rear (RCAL) sections of the calorimeter have a modular structure. Each module is divided into towers. One tower in the BCAL is shown in figure 3.6. The first part of a tower encountered by a particle from the vertex is called the electromagnetic section (EMC). It is divided laterally into four (BEMC,FEMC) or two (REMC) cells each of which are read out by two photomultiplier tubes (PMTs) for more accurate position determination and redundancy. The cross sectional area of a FEMC (REMC) cell is 5 x 20 cm^2 (10 x 20 cm^2), while the BEMC area at the front face is 5 x 24 cm^2. The EMC section is followed by a hadronic section (HAC) which has a cross sectional area of 20 x 20 cm^2 and is further divided longitudinally into two cells in BCAL and FCAL. The BEMC cells are projective in θ and ϕ, the BHAC cells in ϕ only, and FCAL and RCAL cells not at all. Because they are projective in both θ and ϕ, the BEMC cells are the part of the ZEUS calorimeter with the best spatial resolution. There are a total of 5917 cells in the calorimeter, each read out by two PMTs via wavelength shifters. The material of the ZEUS calorimeter has a Moliere radius of $R_m = 2.0$ cm. On average, 90% (95%) of the energy of an electromagnetic shower lies inside a cylinder of radius R_m ($2R_m$).

The natural radioactivity of uranium causes a low, constant background level which is very useful because it enables the PMT gains to be determined on a daily basis. The thickness of the stainless steel cladding surrounding the uranium plates was chosen to reduce the radioactivity to a level that won't significantly interfere with energy measurements, but still allows enough of a signal for calibration purposes. The effect of the uranium signal on physics analysis is reduced by placing minimum energy cuts on the cells: E(EMC) ¿ 60 MeV and E(HAC) ¿ 110 MeV.

3.3.2 Central Tracking Detector

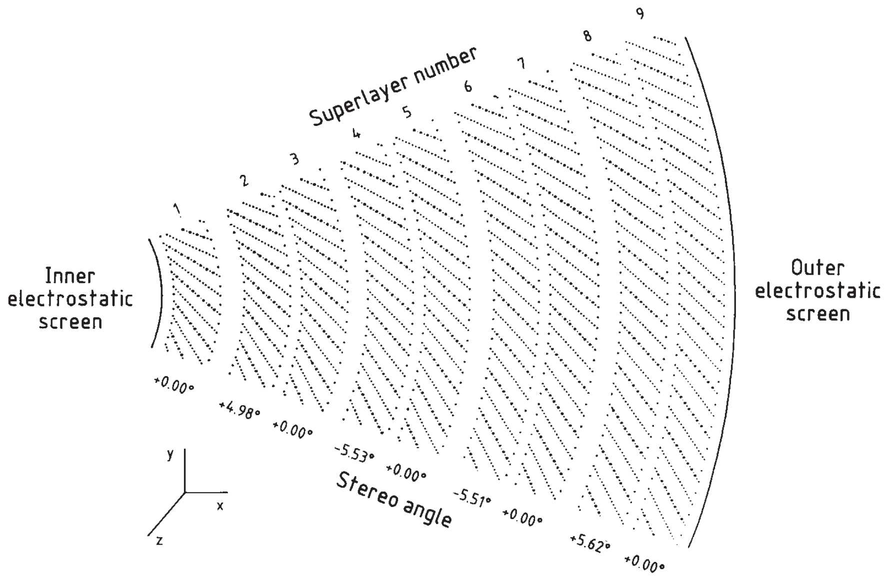

Figure 3.7: Layout of wires in one octant of the Central Tracking Detector.

The Central Tracking Detector (CTD) is a drift chamber consisting of 72 cylindrical layers arranged in nine 'superlayers' Acceptance for reconstructed tracks begins in the angular range $18° < \theta < 161°$ with full acceptance in the range $36° < \theta < 143°$. The active region extends 2.05 m along the z axis and from 18 cm to 79 cm in the radial direction. A gas mixture of Ar/CO_2/ethane (82/13/4) + ethanol fills the entire volume. Argon is used because of the low electric field intensity needed for avalanche formation and its low cost. CO_2 acts as a quencher by absorbing photons to prevent them from starting or extending avalanches. Charged particles traversing the CTD ionize atoms in the gas. The electrons drift in the azimuthal direction at a nearly constant velocity in a uniform electric field, eventually resulting in a measurable signal at the sense (anode) wires.

The layout of wires in one octant is shown in figure 3.7. The sense wires are indicated by the larger dots. The rows of wires between the sense wires are held at varying potentials to create a uniform electric field. The odd-numbered layers have wires strung parallel to the beam axis. To determine the z position of a signal, the even-numbered layers have wires tilted by a small 'stereo' angle of approximately five degrees relative to the beam axis. The azimuthal (ϕ) coordinate of a hit is determined by the time to drift towards the sense wires, while the radial coordinate is given by the location of the wire in which the signal is detected. The CTD measurement of the ep vertex position has a resolution of 0.4 cm in z and 0.1 cm in x,y.

Of vital importance to the prompt photon analysis is the fact that a high energy photon will not leave a track in the CTD. A charged particle such as an electron or positron, which may cause a photon-like signal in the calorimeter, will not be mistaken for a photon because of the track it leaves in the CTD.

3.3.3 luminosity monitor

A measurement of the prompt photon cross section is the ultimate purpose of this work. In order to do this, an accurate knowledge of the integrated luminosity of the data sample is required. This is achieved by the luminosity monitor, shown in figure 3.8. It consists of a photon detector at z = -104 m and an electron/positron detector at z = -35 m, both of which use a lead-scintillator

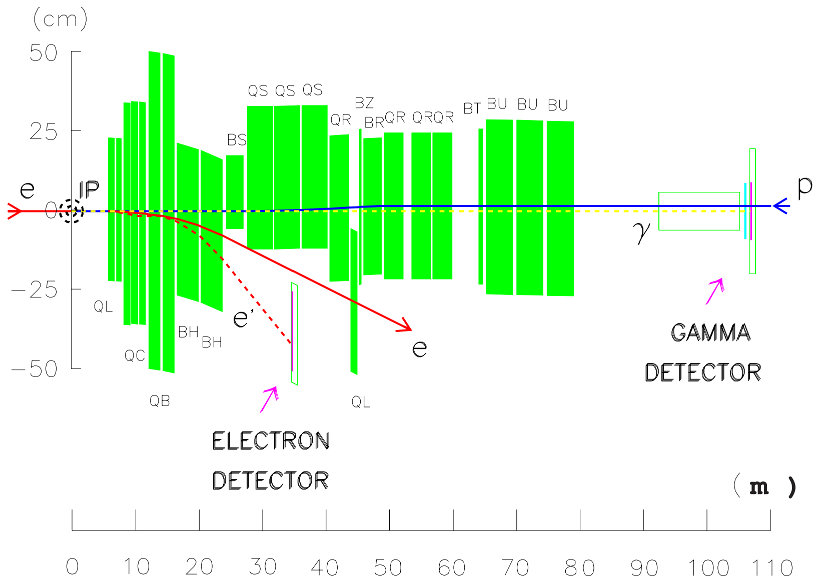

Figure 3.8: Layout of the luminosity monitor. The locations of the electron/positron and photon detectors are shown as well as quadrupole (Q) and dipole (B) magnets.

sandwich calorimeter. The aim is to detect in coincidence the final state electron/positron and photon in the bremsstrahlung (Bethe-Heitler) process $ep \to ep\gamma$. When the beam protons are bent by a magnet, the final state photons leave the proton beam pipe and hit the photon calorimeter. Similarly, electron/positron beam magnets deflect off beam energy electrons/positrons out of the beampipe and into the electron/positron detector. The Bethe-Heitler cross section is well known, so a measurement of the event rate is a measurement of the luminosity.

3.3.4 Small angle Rear Tracking Detector (SRTD)

One of the reasons to build the small angle rear tracking detector at ZEUS was to improve the energy and position measurement of scattered positrons in the rear direction. A measurement using the calorimeter alone underestimates the true energy because the positrons lose energy in inactive (dead) material before entering the calorimeter. The energy lost by a positron in the inactive material is proportional to the number of particles in the resulting shower. Since the SRTD energy deposit is proportional to the number of particles, it can be used to correct the calorimeter estimate of the positron energy. An accurate measurement of positrons near the RCAL beampipe is not critical in the prompt photon analysis itself. The SRTD is used, however, in the independent check of the background due to jets being misidentified as isolated photons as described in section 7.3.

The SRTD consists of two overlapping perpendicular layers of plastic scintillator strips read out by optical fibers and photomuliplier tubes. The detector covers completely the angular range $169° < \theta < 176°$. The 10 mm wide by 5 mm thick scintillator strips provide a positron position resolution of approximately 0.3 cm, much better than the average calorimeter resolution of 1 cm. The energy scale calibration was done using a ^{106}Ru source (before installation in ZEUS) and ep data [11]. The estimated 10% uncertainty in this calibration is acceptable since the SRTD is used only to correct the calorimeter energy for losses due to inactive material. These losses are typically on the order of 10% of the particle energy. Thus the SRTD calibration uncertainty of 10% corresponds to an uncertainty in the particle energy of 1%, which is smaller than the calorimeter energy resolution.

The calculation of the SRTD positron energy correction for the 1995 detector geometry made use of three classes of events in which the positron energy is determined from kinematic constraints: 1) kinematic peak events (low y and low Q^2), in which the scattered positron energy is kinematically constrained to be close to the positron beam energy, 2) DIS ρ° events, $ep \rightarrow ep\rho^\circ$, in which the pair of charged pions from the ρ° decay balance the scattered positron momentum, and 3) elastic QED Compton events, $ep \rightarrow ep\gamma$, in which the photon balances the scattered positron momentum. Using these event samples the scattered positron energy is corrected on average to well within 2% of the true energy, in the range 8 GeV to 27.5 GeV [11]. An added benefit of this correction is an improvement in the measured energy resolution.

3.3.5 Trigger

references?

A bunch crossing every 96 ns at HERA corresponds to a 10.4 MHz input rate for the trigger. A three level trigger system is used to reject background and select potentially interesting ep physics events while reducing the rate by more than a factor 10^6 from 10.4 MHz to about 5 Hz – the rate at which the data is stored. Figure 3.9 shows the flow of data through the three main elements of the ZEUS trigger system - the Global First Level Trigger (GFLT), the Global Second Level Trigger (GSLT), and the Third Level Trigger (TLT). Because of the pipelined, deadtimeless nature of the trigger, data from each new bunch crossing are accepted although the entire trigger decision requires

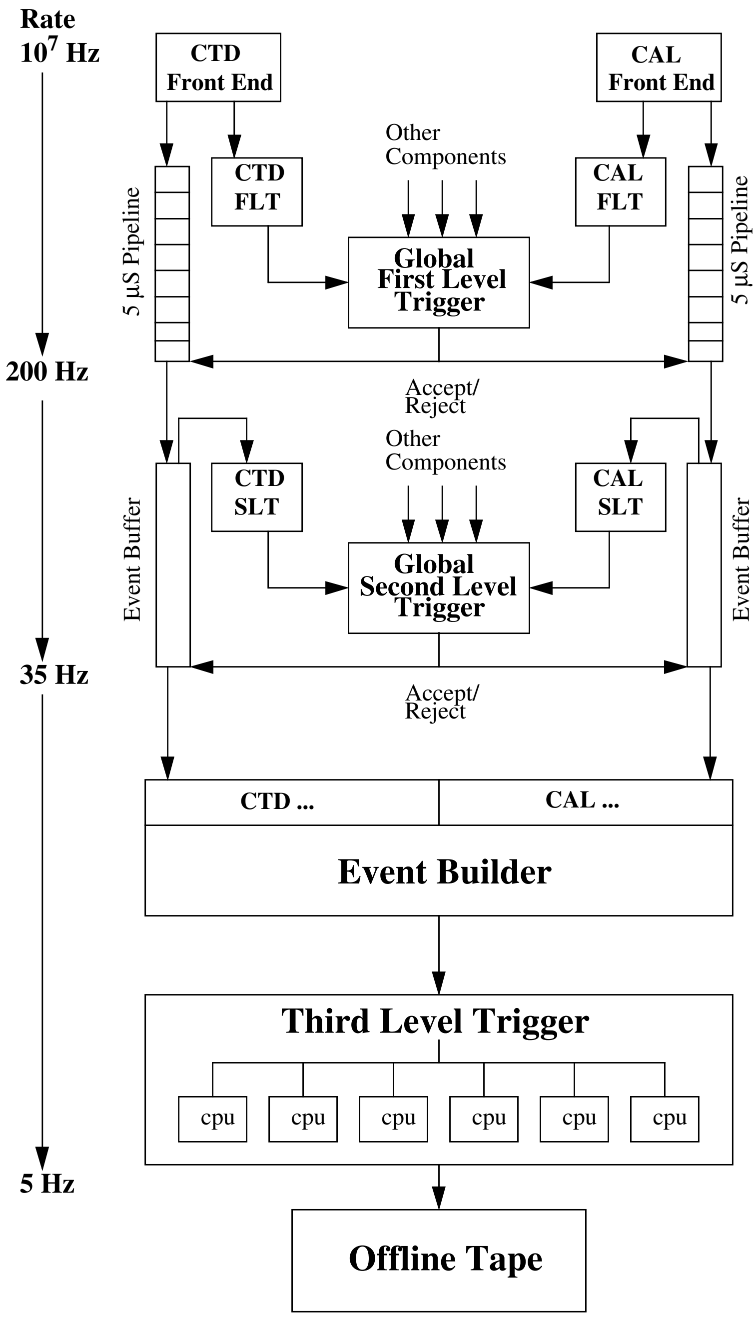

Figure 3.9: ZEUS trigger flow.

approximately 0.3 seconds. Some of the algorithms used at each trigger level to reject background and select physics events are described in section 5.1.

There is a high background rate due to proton beam-gas interactions - protons in the beam colliding with particles in the beampipe vacuum. The task of rejecting this background and determining if an event displays interesting physics characteristics begins with the first level triggers (FLTs) of the various subdetectors of ZEUS: the calorimeter, the Central Tracking Detector, etc. As an example of a first level trigger, the calorimeter FLT is discussed in some detail below. The data of each subdetector are kept in a pipeline while the GFLT hardware combines and processes the FLT information provided by each subdetector, forming 64 subtriggers. The final GFLT decision is the logical OR of the subtriggers. After 4.4μs (46 bunch crossings), the GFLT decision to accept or reject the event is sent to all subdetectors.

If the GFLT accepts an event, the data of each subdetector are sent to the respective SLT for further processing. At the SLT, the data are mostly digitized and more precise than at the FLT. More complicated algorithms can be used to make an accept/reject decision. The GSLT uses transputers [ref] to process the information from the component SLTs resulting in about a factor five reduction in the rate.

If the GSLT accepts the event, data from each component are transferred to the Event Builder which combines and formats it(?) before sending it to the Third Level Trigger (TLT). The goal of the TLT is to reduce the GSLT output rate to about 5 Hz. It achieves this by using a processor farm of Silicon Graphics stations running code which identifies specific physics channels. The

TLT has almost the full off-line data set available to make its decision. The raw data of an event accepted by the TLT are stored on tape and later processed to extract reconstructed physics variables.

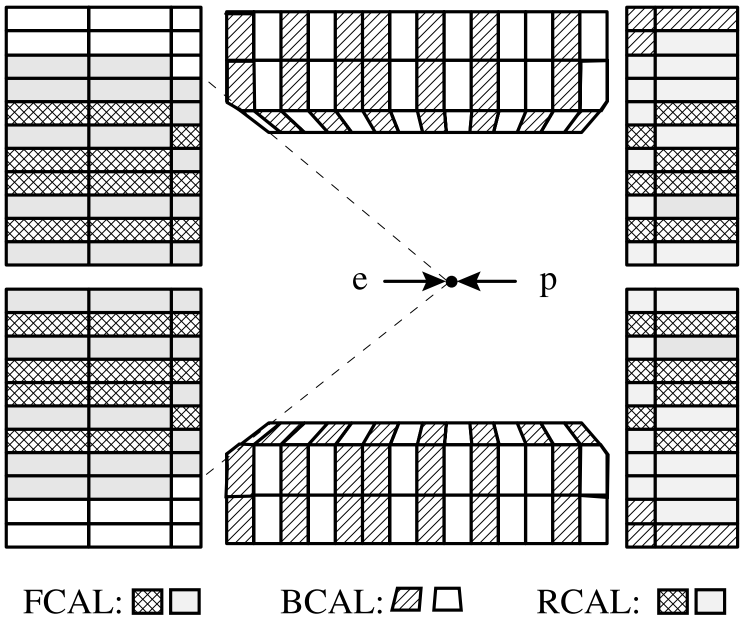

Figure 3.10: Side view of CFLT tower arrangement.

Calorimeter First Level Trigger (CFLT)

The CFLT[15] is very important for rejecting background events such as proton beam-gas interactions in order to reduce the data rate from 10.4 MHz to a more manageable level. As far as the CFLT is concerned, the information from the 5917 calorimeter cells is grouped into 896 trigger towers. A typical tower in the BCAL is shown in figure 3.6. It consists of 4 EMC cells and 2 HAC cells each of which is read out by two photomultiplier tubes, left and right. Analog cards on the detector shape the PMT signals and store them in a switched capacitor pipeline ready to be read out if a first level trigger is received. In addition, the analog card sums together 5% of each PMT signal to produce an EMC sum and a HAC sum for each tower. These sums are sent to the CFLT electronics which begin with the Trigger Sum Card (TSC).

The TSC sums together the left and right signals for each EMC and HAC section. Because of the summing of individual calorimeter cells done by the analog card, the CFLT has much coarser position resolution than the calorimeter, but a more manageable total number of channels. The TSC creates semi-projective trigger towers by combining the signals of adjacent non-projective calorimeter towers where appropriate. Examples of this are shown in figure 3.10 where groups of cells belonging to a single trigger tower are identically shaded.

By means of a serial interface connected to a command cable, the TSC can be programmed to turn off either the left or right side of a trigger channel. If one side is noisy, the signal from this side can be turned off by sending the appropriate serial data to the TSC while the signal of the other side is doubled in a memory lookup table in downstream electronics. The amplification of the trigger signal in the TSC depends on the location of the channel. The maximum expected energy deposit in the FCAL (400 GeV) is larger than that in the BCAL or RCAL (100 GeV) and the gains have been set accordingly. The shaped, amplified pulses are sent as differential signals along 60m of shielded twisted pair cable to the Trigger Encoder Cards (TECs) in the electronics house (rucksack), which contains the remaining CFLT hardware.

The organization of the CFLT is shown in figure 3.11.

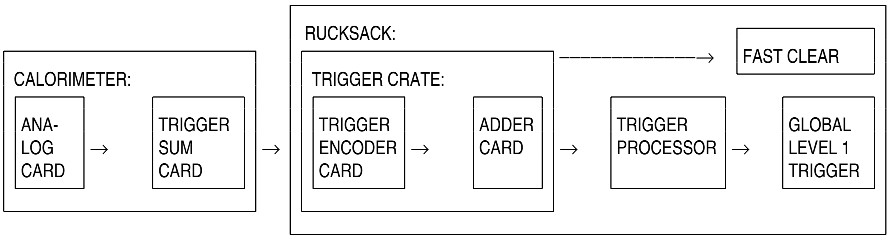

Figure 3.11: Organization of the Calorimeter First Level Trigger

The 224 TECs digitize the EMC and HAC energy sums from the TSCs. Every calculation done in the CFLT electronics, including this digitization, is performed every 96 ns so information from each bunch crossing can be accepted. Using programmable geometric lookup tables, the quantities E_{total}, E_T, E_x, and E_y are calculated for each of the 896 trigger towers. Also, the sum of each of these quantities over all four trigger towers associated with the TEC is calculated. A quiet bit, electromagnetic bit, and muon bit are set for each tower if the tower energy is very small (less than minimum ionizing), consistent with an electromagnetic energy deposit, or consistent with a muonic energy deposit, respectively. Based on the total energy of each tower, the TEC also sets programmable energy threshold bits which form six different threshold values.

Each group of 14 TECs in a single VME crate in the rucksack corresponds to a region in the calorimeter consisting of 56 trigger towers. For each of the 16 regions, there are two adder cards which continue the process of forming energy sums. These cards also use pattern logic to identify isolated electrons and muons.

The adder card sends its data to the CFLT processor (CFLTP) which resides in a separate crate. The CFLTP creates the final global and regional energy sums and determines the final number of isolated electrons and muons by comparing region boundaries. All data from the CFLTP are sent to the GFLT every 96 ns. The total time for the calorimeter first level trigger to do its calculations is 2μsec.

Chapter 4

Monte Carlo

4.1 Monte Carlo use in high energy physics

The term "Monte Carlo" was introduced during World War II as a code word for the secret U.S. development of the atomic bomb at the Los Alamos National Laboratory. (ref?) This work involved the simulation of random neutron diffusion in fissionable material. Since then, the Monte Carlo method has become a powerful technique for analyzing complex problems in a wide variety of fields.

In high energy physics, as in other fields, the Monte Carlo method is used to select variables in a random way, but based on desired probability distributions. Monte Carlo techniques are used in a variety of ways including 1) simulation of physics processes, 2) simulation of detector response and 3) testing analysis strategies.

Physics processes are simulated in computer programs called event generators. The starting point of these programs is generally the collision of two particles. The final result is a list of potentially observable particles each with a specified momentum. Figure 4.1 shows schematically the three stages of a

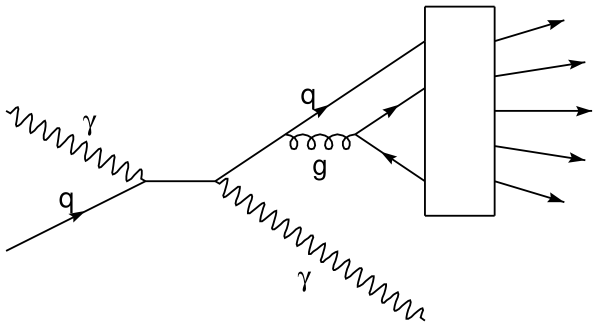

Figure 4.1: The hard subprocess, parton showering, and hadronization of an event generator.

positron-proton interaction using an event generator such as PYTHIA. First there is the hard subprocess. In this example, a photon radiated from the positron interacts with a quark in the proton to produce an outgoing quark and photon. During parton showering, the second stage of the interaction, relatively soft partons develop from incoming and/or outgoing partons. In the example, the outgoing quark radiates a gluon which splits into a quark-antiquark pair. Both the hard subprocess and the parton shower are calculated using perturbative QCD. Finally there is the hadronization stage, denoted by a box in figure 4.1. The term hadronization refers to the transformation of colored partons into colorless hadrons, which can decay creating still more particles. Because hadronization is not understood using first principles, the approach used in event generators is based on models such as the Lund string fragmentation model [8]. In this model, colored partons are connected by strings which break apart creating additional parton pairs. When their mass is low enough, these strings eventually decay into observable hadrons.

A simulation of the signal of a given particle with a given momentum in a detector is another frequently used application of the Monte Carlo technique in high energy physics. What the signal looks like and how often the particle is misidentified or even completely missed by the detector apparatus are questions the Monte Carlo simulation can help to answer. These answers provide a way to estimate detector acceptance corrections which are applied to raw data in order to extract the 'true' physics signal. Being able to simulate physical processes in detectors is also very useful during the design and development stages of new detectors.

The creation and testing of new analysis strategies can be achieved by the use of Monte Carlo methods. These strategies aim to capture a specific physics channel signal and to reduce background. One example is the question of how best to discriminate between a photon and a neutral pion using existing detector components. Various algorithms can initially be tested using Monte Carlo to see which if any can make the required discrimination.

4.2 Monte Carlo used in this analysis

Figure 4.2 shows the ZEUS Monte Carlo chain. Raw data from the ZEUS detector is passed through the ZEPHYR reconstruction program in order to reconstruct physics variables (energy, momentum, etc.) from raw subdetector data. Equivalently, a physics model can be used to generate events which are then passed through the detector and trigger simulations before being reconstructed in the same way as the actual data. To simulate the ZEUS detector and trigger in the 1995 running period, version num95v2.1 of the

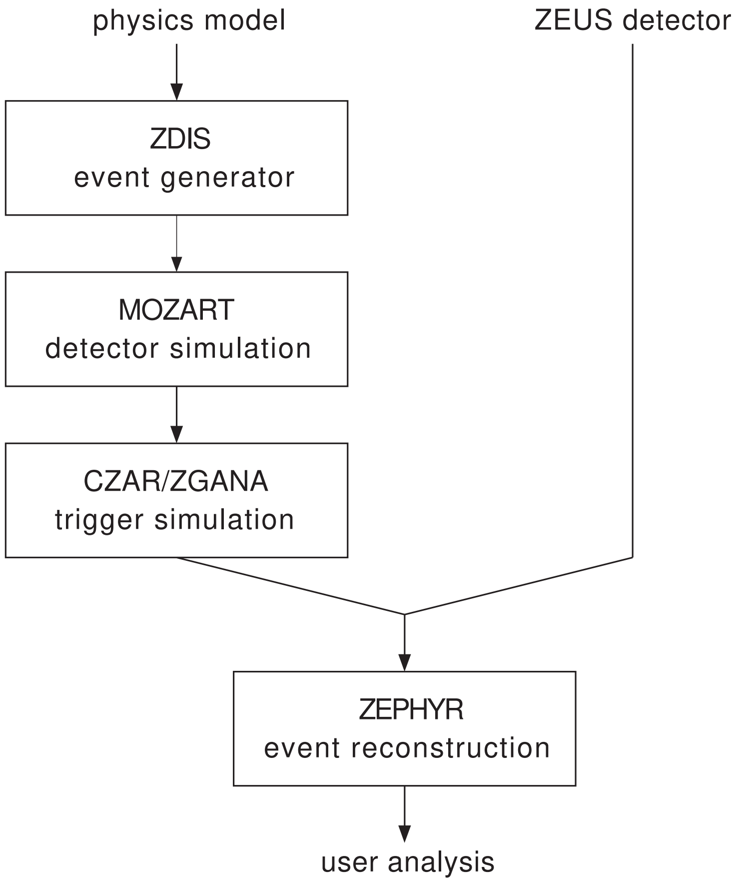

Figure 4.2: ZEUS Monte Carlo Chain

simulation software was used.

Three types of Monte Carlo samples were used in this analysis: 1) the prompt photon process 2) single particles (γ, π°, η) and 3) dijet processes which can mimic a prompt photon final state.

The Pythia-5.7 [6,7] Monte Carlo generator was used to simulate the direct and resolved prompt photon processes and dijet processes. This is a leading order (LO) Monte Carlo program so next to leading order (NLO) contributions to the cross section are missing. The subprocess used to generate events is fermion + photon $\rightarrow$ fermion + photon where fermion = up, down, strange or charm. The MRSA(ref) proton structure function and GRV(LO)(ref) photon structure function were used. The minimum Pt of the hard scatter was set to 2.5 GeV and the maximum Q^2 set to 4 GeV^2. In running PYTHIA initial and final state QCD and QED radiation were turned on. Multiple interactions were not allowed in the resolved event sample since they are not expected to have a significant effect in this analysis.

The equivalent integrated luminosity of the direct and resolved prompt photon Monte Carlo samples is 168.2 pb^{-1} and 169.4 pb^{-1} respectively. The majority of these events passed through an enrichment filter in addition to the cuts mentioned above. This filter required the prompt photon to have Pt $\geq$ 3.5 GeV and $\mid \eta \mid \leq 2.0$. These cuts are a safe distance away from those used in the final analysis and ensure a sample of Monte Carlo events in which a relatively high-Pt photon enters the central part of the ZEUS detector.

To produce a Monte Carlo 'background' sample, direct and resolved dijet events were generated and passed through one of two different enrichment filters. Both filters required the 2 highest Pt jets to have $\mid \eta \mid \leq 2.0$ and Pt $\geq$ 3.5 GeV [current version]. One of the filters further demanded that a final state quark emits a photon with Pt $\geq$ 3.5 GeV and $\mid \eta \mid \leq 2.0$. 39.8 pb-1 of direct dijet events of this type were generated. The other filter demanded that one or more of the jets has at least 80% of its Pt carried by one or more of the following particles: photon, pizero, eta, Kshort, Klong. These particles can mimic a single photon energy deposit in the detector ($\pi^\circ \rightarrow 2\gamma$ (99%), $\eta \rightarrow 2\gamma$ (39%) or $\eta \rightarrow 3\pi^\circ$ (32%), Kshort $\rightarrow 2\pi^\circ$ (31%), Klong $\rightarrow 3\pi^\circ$

(22%)). The particles were chosen after examining dijet monte carlo events which passed all of the prompt photon analysis cuts. 25.4 (20) pb-1 of direct (resolved) dijet events of this type were generated.

Three sets of single particle Monte Carlo samples were generated using JETSET 7.3 (ref): 50000 photons, 50000 pizeros, and 20000 etas. These are not simulated physics events. A single particle is generated at the vertex with a flat energy distribution between 3 and 20 GeV and an isotropic angular distribution. Et-dependent exponential weighting functions were subsequently applied to reproduce the observed Et distributions. These events are essential for the understanding and separation of signal and background using shower shapes in the calorimeter.

Chapter 5

Event Selection

There are several distinguishing characteristics of events in which a prompt photon process (figures 2.2, 2.3) occurs. A high-E_T photon should leave an energy deposit in the electromagnetic sections of the calorimeter. The photon will tend to be rather well isolated from other particles, unlike a photon produced within a jet. There should be a jet opposite the photon. The combination of photon and jet produce significant transverse energy.

characteristics of a prompt photon event — what can we trigger on? isolated high Et photon in central region of detector, high Et jet opposite photon also in central region of detector, tracks from jet, a vertex close to zero. Jet and photon should produce significant Et.

This dissertation is concerned with the photoproduction process, as opposed to deep inelastic scattering (DIS). In photoproduction at ZEUS, the positron is scattered at such a low angle relative to the positron beam direction that it escapes undetected down the beampipe.

What is non physics background? Describe beamgas and halo muon and cosmic ray events...

This chapter describes the online cuts (applied at the trigger level) and offline cuts as well as some physics effects of these cuts. (Data sample is $6.36\mathrm{pb}^{-1}$ integrated luminosity in 1995.)

5.1 trigger (online) cuts

First Level Trigger (FLT)

Detailed calorimeter information is not yet available at the FLT. Regional and global calorimeter energy sums are used for triggering.

The following FLT quantities were used:

E_{tot}	total energy in the calorimeter excluding three rings of towers around the FCAL beampipe and one ring of towers around the RCAL beampipe
EMC_{tot}	same as E_{tot} but only energy in EMC cells is summed
BEMC	total EMC energy in the BCAL
REMC	total EMC energy in the RCAL excluding one ring of towers around the RCAL beampipe
E_T	total transverse energy in the calorimeter excluding two rings of towers around the fcal beampipe, trkveto, goodtrk

[all but 1 of 174 fmax events have slot 42 set (else 41 is set)] What is goodtrk? What is trkveto? What are other vetos? (C5, SRTD, VETOWALL) To be a prompt photon candidate, each event must satisfy at least one of the following conditions:

- ($E_{tot} > 20$ GeV) OR ($EMC_{tot} > 15$ GeV) OR (BEMC > 4.8 GeV) OR (REMC > 3.4 GeV) trkveto

- E_T > 15 GeV (no trkveto cut!)

- (E_{tot} > 15 GeV) OR (EMC_{tot} > 10 GeV) OR (BEMC > 3.4 GeV) OR (remc > 2.0 GeV) trkveto goodtrk

- E_T > 11.6 GeV trkveto goodtrk

Each of these four conditions represents one of the 64 GFLT subtriggers. These subtriggers were not designed specifically to capture prompt photon events – they are effective for many different physics analyses. The logic BEMC > 3.4 GeV is very efficient for the prompt photon analysis since ultimately a photon candidate in the BCAL with E_T^{γ}> 5 GeV is required.

Second Level Trigger (SLT)

There are several cuts at the SLT based on the arrival time of signals in the different parts of the calorimeter. If a positron bunch and proton bunch collide at the nominal interaction point of z = 0, the time measured from the signal in the RCAL, FCAL, or BCAL is exactly zero by definition. This allows the background due to beamgas to be rejected using timing cuts. A proton which collides with a particle in the beampipe vacuum before reaching the ZEUS detector will produce a shower of particles that hit the RCAL approximately 10 ns earlier than the particles from a good ep interaction. A cut of t_{RCAL} > -8 ns is made to reject such events. Similarly, the cuts t_{FCAL} - t_{RCAL} < 8ns and (time from top half of BCAL) - (time from bottom half of BCAL) > -10 ns are made to reduce the background from beamgas and cosmic rays, respectively. Maybe show plot of t_{FCAL} - t_{RCAL} vs t_{RCAL} time.

Mention spark rejection here and global Σ(E-P_z)veto...

Hard Photoproduction High Et SLT filter:

-60 cm $<$ CTD SLT z vertex $<$ -60cm (if there is good ctd slt info)

at least 1 CTD track pointing towards vertex

e-pz gt 8

etbox gt 8

(e-pz gt 12 or pz/e lt 0.95)

Note: vertex (x,y,z) = 0,0,0 is used at SLT.

Explain why these SLT cuts are used...

Third Level Trigger (TLT)

At the third level trigger, raw data from various components is reconstructed so the veto and physics algorithms are able to use meaningful physics quantities. The calorimeter reconstruction is performed at the TLT. Bad channels are taken into account and the energy is zero-suppressed using the following cuts: 60 MeV for EMC cells and 110 MeV for HAC cells. Calorimeter energy sums and energy-weighted times are calculated. The Central Tracking Detector (CTD) reconstruction is performed to produce a list of tracks as well as a vertex postition. After this is done, vertex-corrected calorimeter quantites are calculated (E_T,Σ(E-P_z), etc.).

vetos:

Events are rejected if a spark is identified and the remaining energy in the calorimeter is less than 2 GeV. A calorimeter cell is defined as a spark candidate if there is a large energy imbalance between its two PMTs:

$E_L + E_R > 1.5$ GeV AND $\mid (E_L - E_R)/(E_L + E_R) \mid > 0.9$

where E_L and E_R are the energies of the left and right PMT.

Calorimeter timing is used at the TLT to reject out of time events in a way similar to the SLT timing cuts. A weighted average time is calculated for each of three calorimeter regions: FCAL, RCAL, GLOBAL (the entire calorimeter) using the error on the time of each PMT as the weight factor. To have a time consistent with an ep interaction, an event must satisfy all of the following conditions:

$\mid t_{\mathrm{RCAL}} \mid < 6ns$

$\mid t_{\mathrm{FCAL}} \mid < 8ns$

$\mid t_{\mathrm{FCAL}} - t_{\mathrm{RCAL}} \mid < 8ns$

$\mid t_{\mathrm{GLOBAL}} \mid < 8ns$

If the uncertainty on t_{RCAL}, t_{FCAL}, or t_{GLOBAL} is large the conditions above are relaxed. The cuts on t_{RCAL} and $t_{\mathrm{FCAL}} - t_{\mathrm{RCAL}}$ mainly reject proton beamgas events. The cut on t_{FCAL} is used to reject cosmic muon events and positron interactions with residual gas in the beam pipe.

A muon finder routine (MUTRIG[21]) was used to reject events with a cosmic or beam halo muon. This routine is based on the correlation between the time and position of energy deposits in the calorimeter.

physics filter:

There is a reconstructed CTD vertex satisfying the condition $\mid z_{vertex} \mid < 60cm$.

number of badtracks < 6

A badtrack is a well reconstructed track which is consistent with a beamgas event. It points towards the forward half of the detector ($0.3 < \eta < 3$) and extrapolates back to a beam position z < -75 cm.

$\Sigma(\mathrm{E}\text{-}\mathrm{P_z}) < 75$ GeV

$\Sigma(\mathrm{E}\text{-}\mathrm{P_z}) > 5$ GeV

$\mathrm{E_{T,cone}} > 5$ GeV

A cone algorithm jet finder (EUCTLT) is run. This is a slightly simplified (faster) version of the jet algorithm used offline and described in section 5.2. Two or more jets satisfying the following conditions must be found:

$\mathrm{E_T^{jet}} \geq 4$ GeV

$\eta^{\mathrm{jet}} < 2.5$

The two jet requirement is a safe cut to make because ultimately a jet with $\mathrm{E_T^{jet}} > 4.5$ GeV and a photon with $\mathrm{E_T^{\gamma}} > 5$ GeV are demanded. Both of these objects are found by the jet finder.

The efficiency of the combined FLT, SLT, and TLT requirements is estimated to be 97% for the events of this analysis.

5.2 offline cuts

(Put number of events after each cut or set of cuts. This is a bit complicated since I made an initial preselection using EEXOTIC finder and distance of approach of closest track.)

What were dst cuts for HPP group in 1995?:

```
timing(data only):
          reject if -90 lt Trcal lt -6ns
```

```
        reject if Tr gt -90 and Tf gt -90 and (Tf-Tr) gt 6ns
        time-zvert correlation(data only)
        reject if (there's a vertex) and (Tfcal gt -90)
                  and [(14Tf+zvert) lt -40 or (") gt 40ns]
 timing cuts reject beamgas. MC has no beamgas so you don't need a
 timing cut for the monte carlo.
```

Describe initial preselection using EEXOTIC finder and distance of approach of closest track. [Note: I haven't described the finder yet.]

NOISE95 routine applied. Describe this (refer to Xgamma?)

energy rescaling: 5% in BCAL, 2.5% in RCAL

Cleaning Cuts

$-50cm < z_{vertex} < 40cm$

number of vertex tracks ≥ 3 (remove Comptons)

$\mathrm{Y_{jb}}= \Sigma(\mathrm{E}\text{-}\mathrm{P_z})/\ 2^*\mathrm{E}_e$

$\mathrm{Y_{jb}}> 0.15$ beamgas rejection

sqrt(pxcal**2+pycal**2)/sqrt(etcal) < 2.0 charged current DIS rejection

NC DIS rejection

$\mathrm{Y_{jb}}< 0.7$

Event is rejected if $\mathrm{Y}_e = 1.0\text{-}(1.0/55.0)^*\mathrm{E}_e{}^*(1.0\text{-}\cos(\theta_e)) < 0.75$ for any found em cluster (see below) except the photon candidate. Y_e is low for a DIS scattered positron.

Show plots of $\mathrm{Y_{jb}}$and Y_e.

Electromagnetic shower finder

How does the EEXOTIC electromagnetic shower finder work? Describe it here.

[Get caltru info for all cells with nonzero energy. Order all emc cells, hac0 cells, and hac1 chimney cells (treated as emc) by energy. The number of these cells which have energy greater than 1.0 GeV is the initial value of the number of candidates. The maximum number of candidates is 10. If a candidate is within 0.4 (R = sqrt(delta(theta)**2 + delta(phi)**2) of a higher energy candidate, then don't call it a candidate....]

If eexotic finds more than one candidate in an event, which one do I choose? Describe it here.[...]

$5GeV \leq \mathrm{E}_{\mathrm{T}}^{\gamma} \leq 10GeV$ The 10 GeV upper cut on $\mathrm{E}_{\mathrm{T}}^{\gamma}$is necessary to reject high energy π°s which decay to two photons that cannot be resolved by the BEMC. See section 6.3.

The photon candidate must be fully contained in the BCAL. This is approximately equivalent to the pseudorapidity cut $-0.7 \leq \eta^{\gamma} \leq 1.0$. BEMC spatial resolution is best in CAL because of the small (5x20cm face), projective cells.

Jet finder

Describe EUCELL jet finder here. (cone algorithm,Snowmass Convention) [...] Don't count photon candidate as a jet. Take highest E_{T}EUCELL jet which has $\mathrm{E}_{\mathrm{T}}^{\mathrm{jet}} \geq 4.5$ GeV and $-1.5 < \eta^{\mathrm{jet}} \leq 1.8$

jet must be opposite photon in phi: delta(phi)(photon-jet) $\geq$ 140 degrees

Variable resolutions

How well do I measure E_T^γ, η^γ, ϕ^γ, E_T^{jet}, η^{jet}, ϕ^{jet}, Y_{jb}, x_γ? Is x_γ defined yet? Show some plots.

5.3 physics effects of cuts

How do the cuts affect/restrict the physics I can do with prompt photons? Example: how much is 'resolved' contribution suppressed relative to the 'direct' contribution by my choice of cuts? Discuss study using generator level cuts in monte carlo.

Chapter 6

Identifying Isolated Photons

The main background in the search for prompt photon events is due to dijet events (figure 2.4 and figure 2.5) because the cross section for dijet processes is much larger than the prompt photon cross section. One need only replace the outgoing photon in a prompt photon diagram with a gluon to get a dijet process. The cuts described in section 5.2 (offline cuts) do not distinguish well between the prompt photon process and the dijet process. This chapter discusses how the dijet process and other backgrounds which survive the previous cuts are rejected.

The dijet process can be a serious background if one jet's energy is carried mostly by a neutral meson such as a π° or η. If a final state quark in a dijet process radiates a high-$\mathrm{E_T}$photon, the resulting final state can also look like a jet plus an isolated photon. A smaller contribution to the background comes from DIS events in which the scattered positron is misidentified as an isolated photon. This background is greatly reduced by the $\Sigma(\mathrm{E}\text{-}\mathrm{P_z}) < 0.7$ cut and the Y_e cut described in section 5.2.

Information from the BCAL and CTD are used to make an energy isolation and track isolation cut. In addition, the shape of the electromagnetic shower in the BCAL is used to reject events in which a neutral meson such as a π° or η mimics an isolated photon. One of the shower shape quantities, Fmax, is used for the statistical background subtraction procedure.

6.1 energy isolation cone

From the prompt photon diagrams in figure 2.2 and figure 2.3, one can see that the final state photon is relatively well isolated, particularly in the direct prompt photon process. A photon produced as part of a jet will not, in general, be as well isolated.

An isolation cone was imposed around the photon candidate: within a cone of unit radius in (η, ϕ), the total $\mathrm{E_T}$from other particles was required not to exceed $0.1\mathrm{E}_\mathrm{T}^\gamma$. This was calculated by summing the $\mathrm{E_T}$in each calorimeter cell within the isolation cone. Additional contributions were included from CTD tracks which started within the isolation but curved out of it. The small number of tracks which curved into the isolation cone were ignored. This isolation condition greatly reduces the dijet background by removing the large majority ($\approx$80%) of events where the photon candidate is associated with a jet, and is therefore either hadronic in origin or else a photon radiated within a jet. In particular, as discussed by previous authors [1,2], it removes most dijet events in which a photon is radiated from a final state quark. The losses of direct and resolved prompt photon events due to the energy isolation condition were found from monte Carlo studies to be $\approx$5% and $\approx$17% respectively. Overall, the isolation condition removed 70% of the candidates remaining at this stage, leaving 568 events [are these numbers correct? Be careful with order of cuts].

[mention what happens when this rather hard 1.0 isolation cone cut is varied.]

6.2 track isolation

A photon candidate was rejected if a CTD track pointed within 0.3 units (in η,ϕ) of it. Say more about this.

6.3 shower width in CAL

The π° and η neutral mesons have a larger shower width in the BCAL because they decay to multiple photons. The relevant decay modes and the branching ratios are given below:

$\pi^\circ \rightarrow 2\gamma$ (99%)

$\eta \rightarrow 2\gamma$ (39%)

$\eta \rightarrow 3\pi^\circ$ (32%)

The opening angle of the two photons from the decay of a π° or η is

[Give formula for angle betwen the two photons in the π° decay...]

In the 5 to 10 GeV $E_T$range used in this analysis, the opening angle of the two photons from a neutral meson decay is about the same as the resolution of the 5x20 cm BEMC cells in the z direction (give numbers). η has wider shower because its mass is much larger than the mass of the π°.

The search for some quantity to distinguish photons and π°s/ ηs on an event by event basis was unsuccessfull because all of the decay products of a π° or η are sometimes contained within a single calorimeter cell. A statistical subtraction of this neutral meson background had to be done using the best available discriminating quantities.

A typical high-$E_T$photon candidate in the BEMC consists of a cluster of 4-5 cells selected by the electron finder. Two shape-dependent quantities were studied in order to distinguish photon, π°, and η signals. These are the energy weighted width of the BEMC cluster in the z direction (Zwidth) and the fraction of the photon candidate energy found in the most energetic cell in the cluster (Fmax).

The shower shape quantity Zwidth is given by the formula

[give formula here...]

i: cells attached to photon candidate (according to the finder)

E_i: energy of cell i

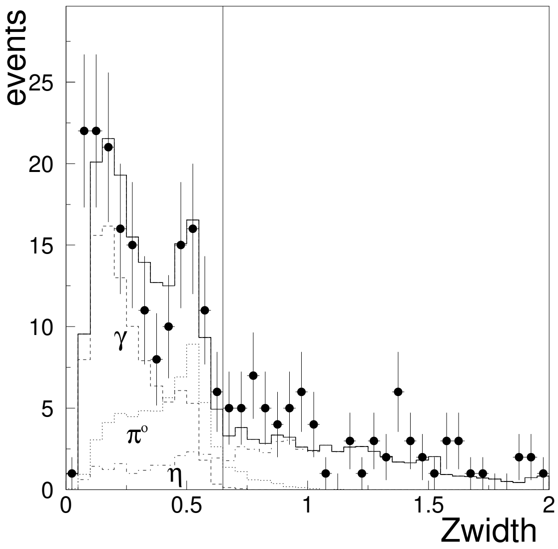

Figure 6.1: Distribution of Zwidth for prompt photon candidates in the data (points) and γ, π°, η fitted Monte Carlo.

In figure 6.1 the Zwidth quantity is shown for the data and three types of single particle Monte Carlo: γ, π°, and η. Zwidth is plotted in units of BEMC cell width. A value of 0.0 means the energy is all in one calorimeter cell. A value of 0.5 means the energy is more or less evenly distributed in two cells. The photon curve peaks at low values of Zwidth ($\approx$) while the two photons from the decay of the π° causes the π° curve to peak at about 0.5. The higher mass and multiple decay modes of the η result in a very broad Zwidth distribution which forms most high Zwidth tail. Events with Zwidth > 0.65 were rejected because there is no photon signal above this value. 174 events remain after this cut.

The second shower variable is Fmax and is defined in the following way:

Fmax = cellemax/etot ...

Figure 6.2 shows Fmax for prompt photon candidates in the data (points) and γ, π°, η Monte Carlo. Only events which have Zwidth < 0.65 are in this plot. The data has a peak at high values of Fmax, corresponding to an energy deposit with a narrow shower width. The π° and η Monte Carlo distributions are broader and extend down to lower values of Fmax corresponding to a larger shower width. A calorimeter deposit in which all the energy is evenly distributed between two cells would have a value of 0.5 for Fmax. It is important to note that the Fmax shape for π°s and ηs is very similar. The background subtraction procedure described below is based on the Fmax quantity and is not sensitive to variations in the ratio of π°/η because the two Fmax shapes are similar.

The peak of the Fmax curve for data does not lie directly on the peak of

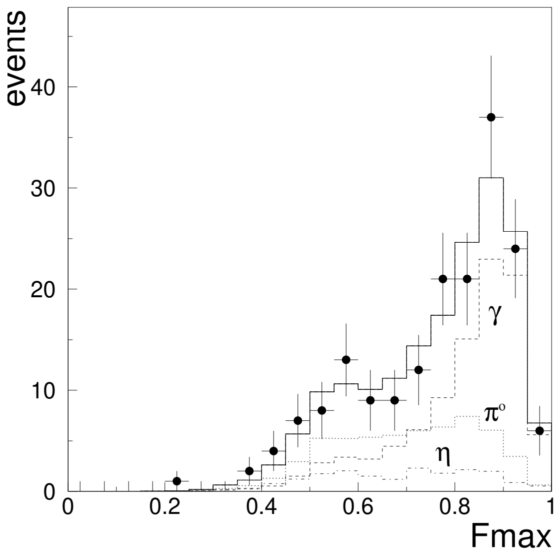

Figure 6.2: Distribution of Fmax for prompt photon candidates in the data (points) and γ, π°, η fitted Monte Carlo.

the Fmax curve for single photon Monte Carlo. In figure 6.2 each of the single particle Monte Carlo curves has been multiplied by 1.025 to get the best fit of the peak. This 1.025 correction factor was determined using a sample of 1995 high Q^2 neutral current DIS events in which the scattered positron went into the BCAL. These positrons should have the same Fmax shape as the single photon Monte Carlo because both the positron and photon should cause an electromagnetic shower in the calorimeter. No clean sample of high-$E_T$photons in ZEUS data could be found. Positrons in the DIS sample which were found by the EEXOTIC finder and have an $E_T$between 5 and 10 GeV were used. The DIS positron $E_T$distribution is almost completely flat in this $E_T$range so it was E_T-weighted (exp(-0.375*Et)) before Fmax was plotted. A track within

10 cm of the EEXOTIC cluster (at the face of BCAL) was required.

The top left [number the different plots] plot in figure 6.3 shows Fmax (cellemax/etot) for these positrons (full circles). Also shown is Fmax for single photon Monte Carlo (open squares) Just like the positrons, the photons are between 5 and 10 GeV $E_T$and are weighted acc. to exp(-0.375*Et) from an initially flat $E_T$distribution. The errors on the photon points are very small. The plot shows that there is general agreement between the shower width for positrons in the data and photons in the Monte Carlo, but the peak of the Monte Carlo photons is at slightly smaller values of Fmax than the positron data.

Figure B shows the same data as figure A (filled circles). The open squares in Figure B show the effect of multiplying the monte carlo photon Fmax by 1.01.

Figure C shows the same data as figure A (filled circles). The open squares in Figure C show the effect of multiplying the monte carlo photon Fmax by 1.02. Figure D shows the same data as figure A (filled circles). The open squares in Figure D show the effect of multiplying the monte carlo photon Fmax by 1.03.

The best matching of the peak is achieved when the photon monte carlo Fmax is increased by 2

chi square fit shows 1.025 factor is best.

check reliability of Monte Carlo using data (π° check is Kensei's work)

laze picture?

What should the high energy cut be for the $E_T$of the photon? At higher

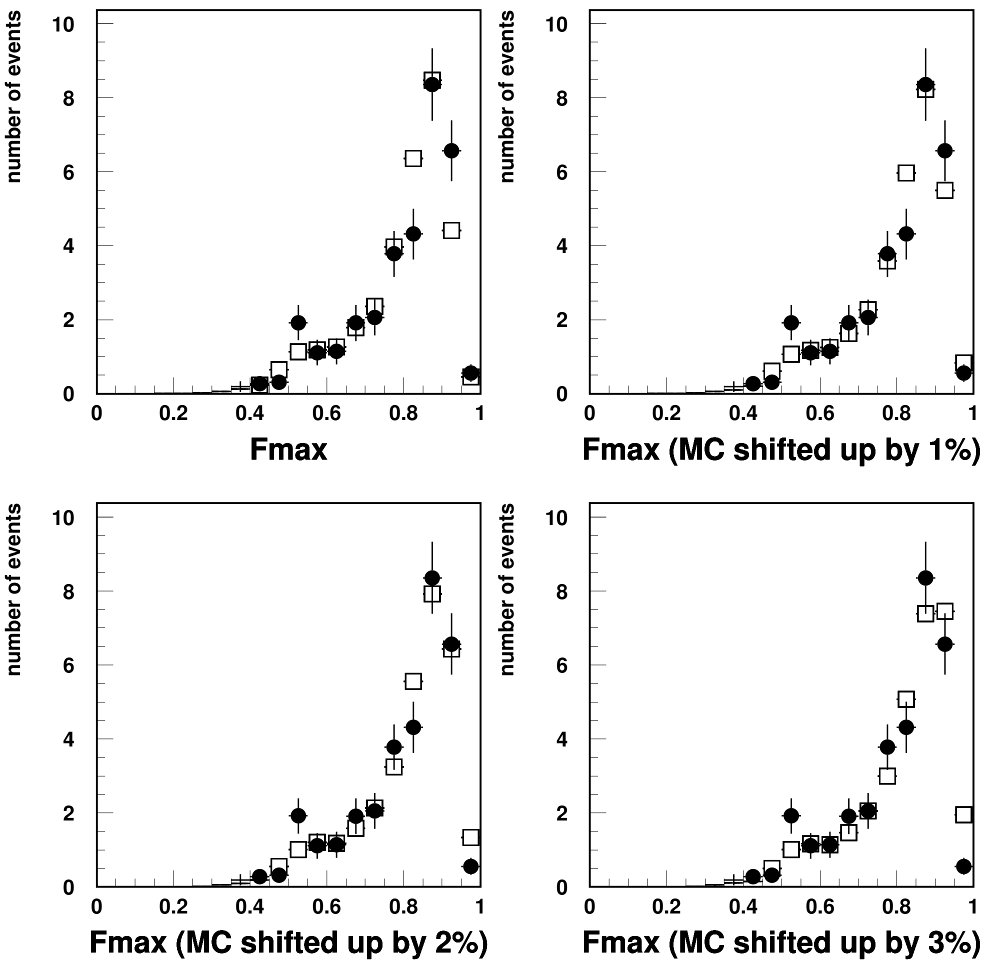

Figure 6.3: A comparison of Fmax for Monte Carlo photons and data positrons.

E_Ts it becomes difficult to separate a single photon and a π° based on the shape of the Fmax curve.

Look at Fmax for single photon monte carlo (filled circles) and single π° monte carlo (open squares) in bins of E_T. The single particle monte carlo has passed many of the analysis cuts: z vertex position, tracking isolation, 10% isolation cone, contained fully in BCAL, dz ¡ 0.65, eexotic electron found. Also, there is an $E_T$weighting done to adjust the flat $E_T$distribution to a more realistic one. All curves have been normalized to have the same area. A shift of 1.025 has been applied.

Five bins of Et are shown: 5.0 - 7.0 GeV 7.0 - 8.5 GeV 8.5 - 10.0 GeV 10.0 - 11.5 GeV 11.5 - 13.0 GeV

In the first two bins the π° s have a much flatter distribution than the photons. In the last bin (11.5 - 13 GeV) the two curves already look similar making a background subtraction at this energy less feasible. In the range 8.5 GeV to 11.5 GeV the PIzero distribution begins to develop a peak at high Fmax similar to the photon distribution. A cut of 10 GeV was chosen for this analysis.

6.4 background subtraction procedure

- describe fitting method (fit is best with ALL 3 single particle MCs)
- get 'signal' and 'background' subsamples

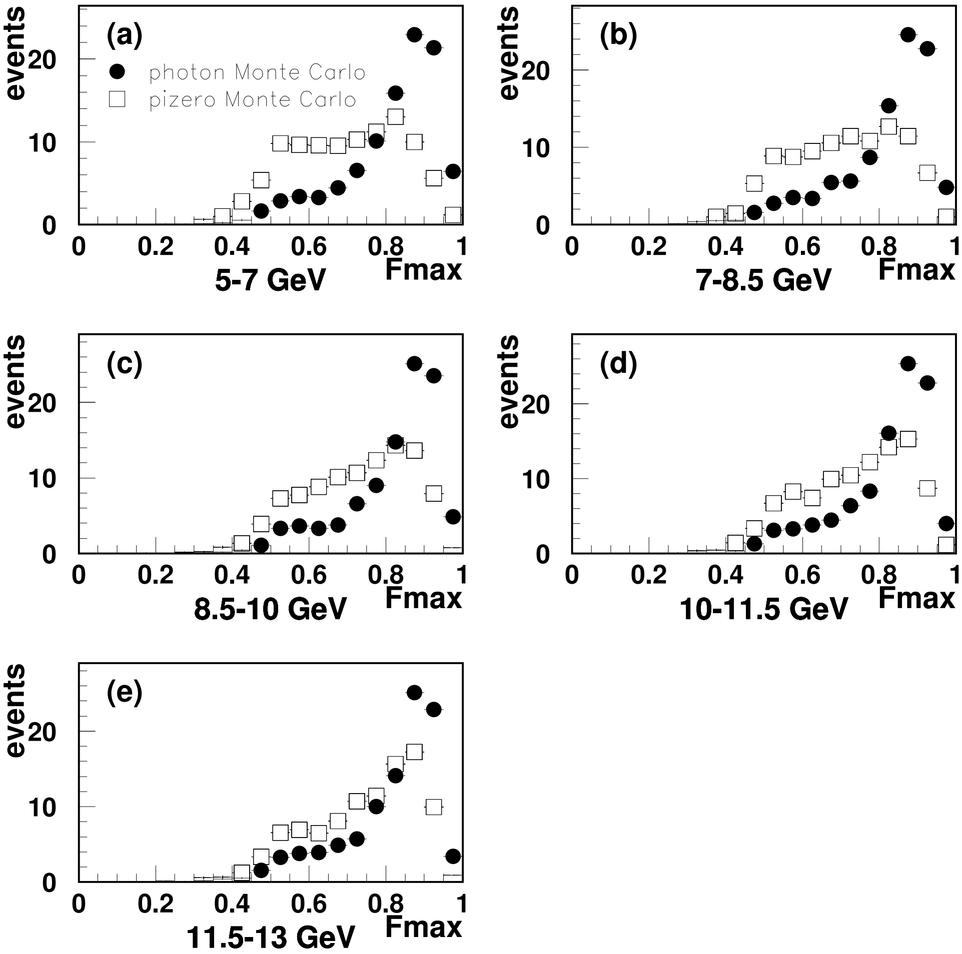

Figure 6.4: A comparison of Fmax shape for single photon and single π° Monte Carlo. Five different bins of photon or π° transverse energy are shown. All curves are area normalized for shape comparison.

Chapter 7

Results

7.1 Xgamma

- how 'measured Xgamma' is defined
- compare Xgamma(meas) plot with LO Monte Carlo (include Krawczyk's numbers?)
- Are we really seeing resolved photons? (Ercal vs. min(photon rapidity, jet rapidity))

7.2 cross section

- definition
- correction factor (to hadron level)
- (efficiency to find the 'cross section definition events' versus my favorite variables)
- systematic errors

- compare with L. Gordon's NLO parton level results
- mention Peter's and Kensei's similar results ('independent' checks)

7.3 independent check of background

In this prompt photon analysis, there is much background due to photoproduction dijet processes (figures 2.4 and 2.5) in which one of the jets creates a calorimeter energy deposit which passes all of the prompt photon cuts. A high E_T jet, for example, can produce a high E_T π° which has a shower profile in the calorimeter very similar to a single photon. The resulting final state looks like a photon plus a jet. An estimate of the magnitude of this background was obtained by comparing calorimeter shower shapes in the prompt photon data sample with γ, π°, and η Monte Carlo shower shapes using the Fmax variable as described in sections 6.3 and 6.4. Although the accuracy of the Monte Carlo shower shapes was reasonably verified with actual data (section 6.3), an independent check of this background using a completely separate data sample would improve the analysis.

The goal, then, is to determine the probability that one of the jets in a dijet process will produce a fake prompt photon signal. A source of jets with a known energy and angular distribution would be ideal for this background check. Fortunately, at HERA, such a data sample exists in the form of Deep Inelastic Scattering (DIS) events (figure 2.6). Using conservation of energy and momentum, the energy and angle of the hadronic activity in a DIS event can be calculated once the energy and angle of the scattered positron has been measured. The hadronic activity will be mainly in the form of the struck quark. The probability, 'photon/jet', that the jet of particles produced by the quark creates a photon-like signal in the calorimeter, within a given transverse energy and pseudorapidity range, can be measured as a function of transverse energy. This probability can then be multiplied by the number of jets which survived the initial prompt photon cleaning cuts (section 5.2) to yield an independent estimate of the background due to jets being misidentified as single photons. This is summarized by the formula

$$number\ of\ background\ events = (number\ of\ jets) \times (photon/jet)$$

The 'number of jets' quantity in the formula is determined by counting the dijet events in the 1995 data sample which pass all cuts of the prompt photon analysis except those cuts used to identify an isolated photon – electron/photon finder, E_T isolation cone, track isolation cone, and shower shape cuts. The total background cannot be larger than this number. These cuts ensure that at least one of the two jets is in the BCAL and satisfies $5 \leq E_T^{jet} \leq 10$ GeV. In 40% of these events, the other jet is also in the proper transverse energy and pseudorapidity range to mimic a prompt photon. The $E_T^{jet} \leq 10$ GeV upper cut was relaxed to $E_T^{jet} \leq 11$ GeV to take into account the possibility that an 11 GeV jet can produce a photon signal between 5 and 10 GeV and still barely pass the 90% E_T isolation cone cut.

A factor 1.14 was applied to the calorimeter level jet E_T to produce the hadron level jet E_T, which is more directly comparable to the E_T of the struck quark in a DIS event. The number 1.14 was determined using a sample of Pythia prompt photon Monte Carlo events. Each calorimeter level jet with

$E_T^{jet} \geq 4$ GeV and in the range -1.5 $\leq \eta^{jet} \leq$ 1.5 was compared to its matching hadron level jet and found to have an average of 14% less transverse energy. This is mainly due to energy loss in uninstrumented material in front of the calorimeter.

The number of jets in the 1995 data sample which could possibly mimic a prompt photon signal is given in three bins of E_T in the following table:

E_T (GeV)	5–7.5	7.5–10	10–12.5
number of jets	19187	17695	8559

The E_T bin width was chosen as small as possible while keeping in each bin at least 10 events in the numerator of the 'photon/jet' ratio. Thus the low statistics of the DIS sample prevents finer binning. To determine the background contribution from each bin, the number of jets must be multiplied by the probability that a jet in that bin will mimic a single photon signal. The method of obtaining this probability from DIS events is discussed in the remainder of this section.

In order for this background check to be feasible, the jet produced by the struck quark in a DIS event must sometimes have $E_T \geq 5$ GeV and pseudorapidity within the BCAL. Unfortunately, most DIS events do not produce such a jet. This can be seen in figure 7.1. In the majority of DIS events the positron scatters at a small angle relative to the original positron beam direction (180°) because this corresponds to low momentum transfer (low Q^2) between the incident positron and proton. The jet will have $E_T \geq 5$ GeV only for positron scattering angles of 170° or less. Although DIS events are plentiful at ZEUS, most of them cannot be used for this study because the jet does not have the

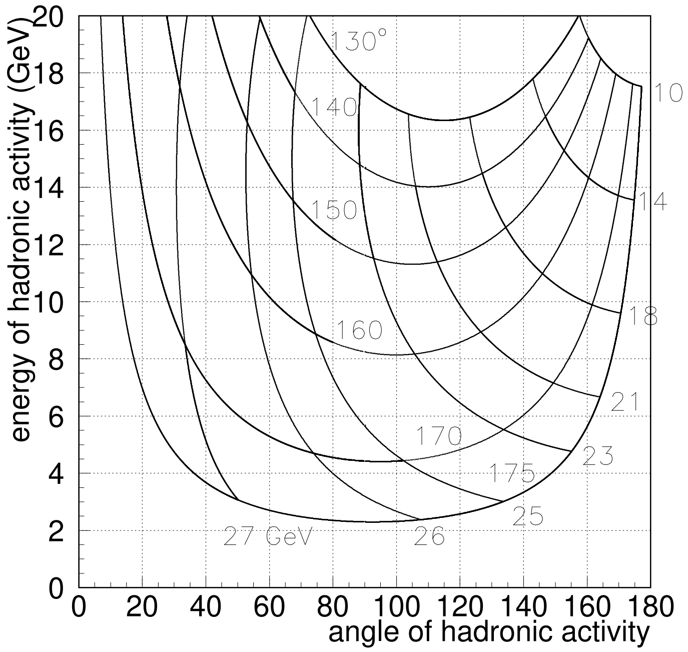

Figure 7.1: (a) Energy vs. angle of hadronic activity in a DIS event with lines of constant energy and angle of the scattered positron shown. An angle of 180° is the original positron beam direction.

required minimum E_T.

The BCAL covers the angular range $37° \leq \theta \leq 129°$. Figure 7.1 shows that events in which the scattered positron energy is less than about 15 GeV cannot have a jet pointing toward the BCAL. Similarly, if the scattered positron energy is greater than about 27 GeV, the event cannot be used for this background study.

The DIS sample consists of data taken in 1995 and 1996 and corresponds to an integrated luminosity of 12.44 pb^{-1}. The following cuts are used to obtain clean DIS events:

- -40 cm $\leq$ CTD $Z_{\mathrm{vertex}} \leq$ 40 cm

- $E_{\mathrm{photoncal}} \leq 1$ GeV

  The requirement of little energy, $E_{\mathrm{photoncal}}$, in the photon calorimeter of the luminosity monitor helps to remove initial state radiation (ISR) events in which the incoming positron radiates a photon. In these events the calculation of the energy and angle of the hadronic activity is incorrect because the original positron momentum is no longer equal to the beam momentum.

- 40 GeV $\leq \Sigma(E\text{-}P_z) \leq$ 60 GeV

  A DIS event in which the scattered positron and jet deposit all their energy in the calorimeter will have $\Sigma(E\text{-}P_z) \approx$ twice the positron beam energy = 55 GeV. This cut helps to remove background due to photoproduction.

- positron with $E \geq 15$ GeV found in RCAL

  The positron identification algorithm (SINISTRA95) is based on a neural network using calorimeter energy deposits [10].

The scattered positron is tagged in one of two ways. The positron can produce a 'good hit' in the small angle rear tracking detector (SRTD) (section 3.3.4). A 'good hit' is well contained within the SRTD and matches the location of the RCAL energy deposit associated with the positron. A box cut of 14 cm $\times$ 14 cm is made using the SRTD (x,y) position. Events in which the scattered positron is inside this 14 cm $\times$ 14 cm box around the beampipe are not available because they are rejected at the trigger level. The calorimeter energy of SRTD tagged positrons is corrected based on the amount of energy deposited in the SRTD. Alternatively, an event is included in this background study if the scattered positron has a matching CTD track associated with it. A matching track must hit the RCAL face within 5 cm of the positron energy deposit and have hits in both superlayer 1 and 2 of the CTD. For these CTD tagged positrons, the cut $\theta_{\rm positron} \leq 165°$ further ensures a good quality track.

The measured energy and angle of the scattered positron is now used to calculate the expected transverse energy ($E_{T,had}$) and angle (θ_{had}) of the hadronic activity. This calculation has an uncertainty mainly due to the calorimeter energy resolution.

In order to study the resolution of $E_{T,had}$ and θ_{had}, 170,000 events corresponding to an effective integrated luminosity of 0.72 pb^{-1} were generated using DJANGO 6.24 [16] which is an interface of the Monte Carlo programs HERACLES 4.5.2 [17] and LEPTO 6.5 [20]. Figure 7.2(a) shows that the measured $E_{T,had}$ is well correlated with the true $E_{T,had}$. Here, 'true' means the generated values of the scattered positron energy and angle are used to determine $E_{T,had}$ and θ_{had}. Similarly, 'meas' means the measured values of the scattered positron energy are used. Figure 7.2(b) shows that measured $E_{T,had}$ is 0-5% smaller, on average, than true $E_{T,had}$. The correlation of true and measured θ_{had} is shown in figure 7.2(c). ISR events contribute to the tendency for true θ_{had} to be smaller (more in the forward direction) than measured θ_{had}. Figure 7.2(d) shows that measured θ_{had} is 0-7° larger, on average, than true θ_{had}.

The shifts in the Monte Carlo between the true and measured values of

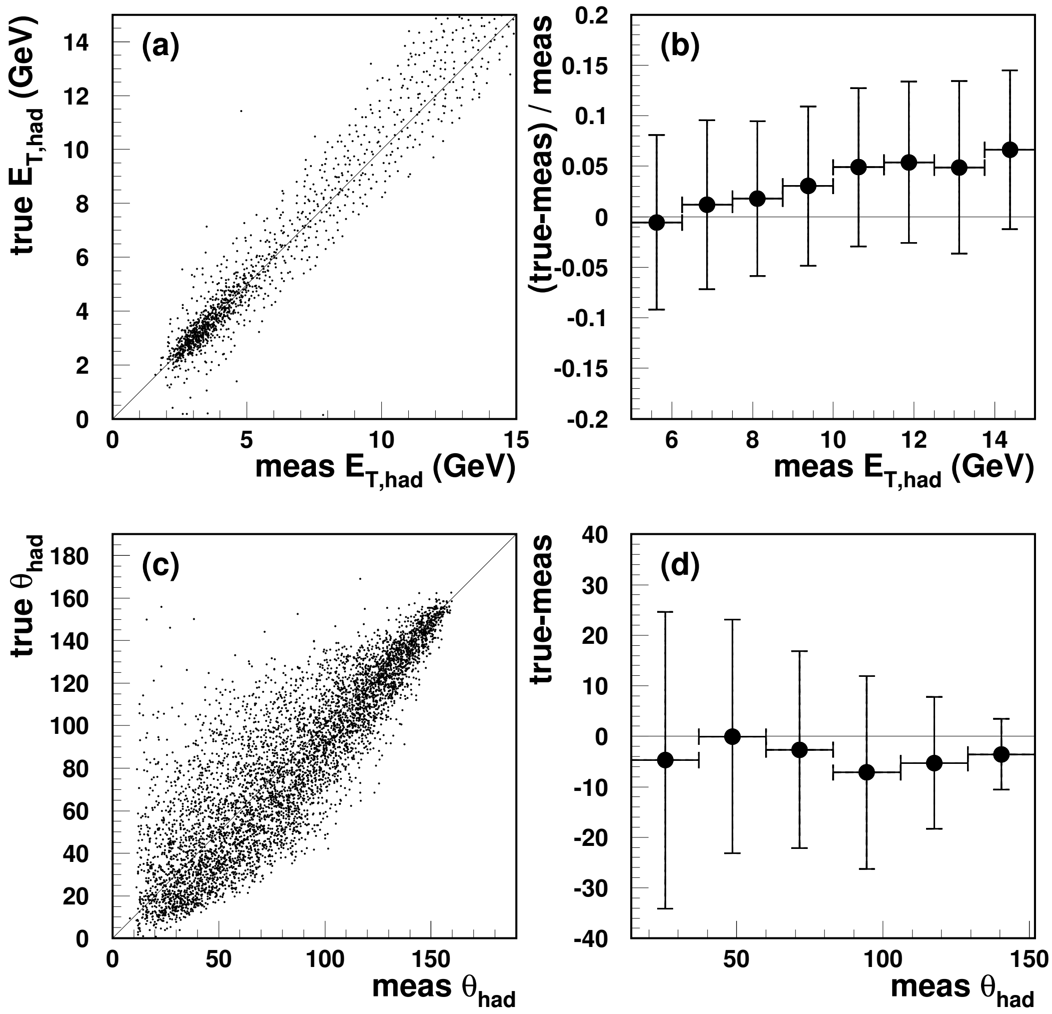

Figure 7.2: The $E_{T,had}$ resolution as determined using the DJANGO Monte Carlo simulation. (a) Correlation of true and measured $E_{T,had}$ (b) The fractional difference between true and measured $E_{T,had}$ showing the mean shift (point) and the sigma of the Gaussian fit (error bar). (c) Correlation of true and measured θ_{had} (d) The absolute difference between true and measured θ_{had} in degrees.

$E_{T,had}$ and θ_{had} are used to correct the measured quantities before the following cuts are applied: $40° \leq \theta_{had} \leq 126°$ and $E_{T,had} \geq 5$ GeV. These cuts require the jet produced by the struck quark to point towards the BCAL with the same E_T cut as for the photon in the prompt photon analysis.

After the DIS cleaning cuts (-40 cm $\leq$ CTD $Z_{vertex} \leq$ 40 cm and $E_{photoncal} \leq 1$ GeV and 40 GeV $\leq \Sigma(E\text{-}P_z) \leq$ 60 GeV and a positron with $E \geq 15$ GeV found in RCAL), the requirement of a good SRTD hit or a matching CTD track, and the cuts on $E_{T,had}$ and θ_{had} are applied, it is interesting to determine how much energy is actually seen where the kinematics predict the jet to be. Figure 7.3(a) shows Ehadfrac, the fraction of the expected energy E_{had} found inside a cone of 1.0 centered at the expected position θ_{had},ϕ_{had} for DIS data. In this plot, the jet is seen as a broad peak between 0.5 and 1.0. In other words, a large amount of energy is seen where it is expected. A striking feature of the plot is the large number of events at zero which indicate that no calorimeter energy was found in the expected position. According to DIS Monte Carlo, which reproduces the Ehadfrac shape in the data very well, the large peak at zero can be attributed to two things: 1) a mismeasurement of the scattered positron energy due to resolution effects and 2) ISR events, in which the event kinematics change because the radiated photon lowers the energy of the incident positron. In both cases, measured θ_{had} is different than true θ_{had}. In order to reject these events the cut Ehadfrac ≥ 0.5 is applied.

Approximately 45,000 events remain after all cuts above have been applied to the 1995 and 1996 DIS data sample. These events form the denominator of the 'photon/jet' fraction. The numerator is the subset of these which pass

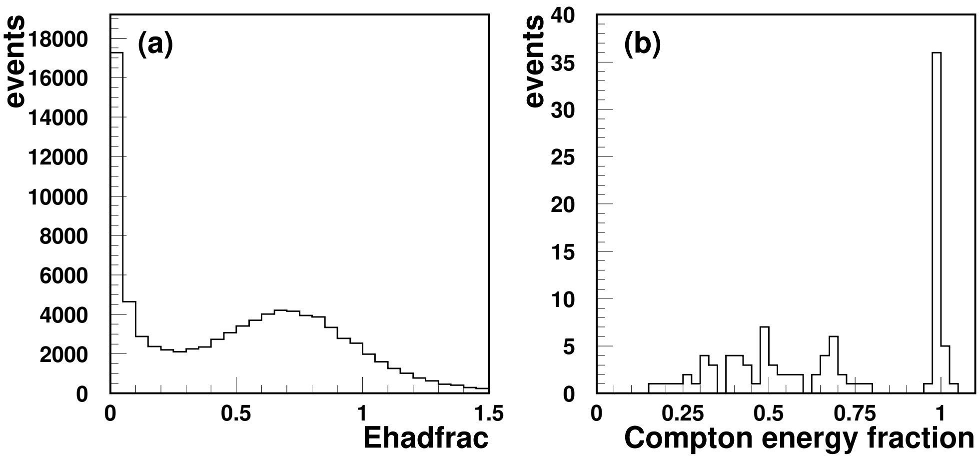

Figure 7.3: (a) fraction of expected hadronic energy found at the expected location (b) fraction of total calorimeter energy contained in the two largest electromagnetic clusters

all cuts of the prompt photon analysis used to identify an isolated photon (described in chapter 6): electron/photon finder, E_T isolation cone, track isolation cone, and shower shape cuts. 102 events pass these cuts but many of them are not useful for this study because they are elastic QED Compton events, $ep \rightarrow ep\gamma$. In such events, the object in the BCAL is actually a photon and not a jet produced by a quark. Since elastic QED Compton events have only two energy deposits in the calorimeter, the scattered positron and the photon, they are easily rejected by the following cut: $(E_{positron} + E_\gamma) / E_{TOT} \leq 0.95$. This quantity is shown in figure 7.3(b). DIS events typically have significant energy not associated with the photon or scattered positron, unlike elastic QED Compton events. This is mainly due to the often large energy deposits from the proton remnant in the FCAL.

After the cut to remove elastic Comptons, 59 events remain. There is still contamination from inelastic QED Compton events in which the proton does not remain intact. Like its elastic counterpart, this type of event should be rejected since the object in BCAL is actually a photon and not a jet produced by a quark. The FCAL energy deposit makes the inelastic Compton process difficult to distinguish from legitimate DIS events on an event by event basis. Therefore a statistical subtraction is done using the inelastic Compton process in the DJANGO6 Monte Carlo program. An event sample corresponding to an effective integrated luminosity of 63.5 pb-1 was generated using this Monte Carlo. Applying all cuts on this sample, it was determined that of the 59 events forming the numerator of the 'photon/jet' fraction, the number due to the inelastic Compton process is 8% to 30% depending on the E_T bin. As a check, the number of events subtracted was increased and decreased by 50% with a less than 10% effect on the final result.

The probability that a jet will mimic an isolated photon in the detector depends on the transverse energy of the jet. The photons from the decay of a neutral meson become more difficult to resolve in the calorimeter as their energy increases. A π° with $E_T > \sim 10$ GeV looks similar to a single photon in the calorimeter, as shown in figure 6.4. It is important that the shape of the E_T distribution in the DIS sample agrees with the photoproduction dijet sample. The 'photon/jet' fraction was adjusted for a disagreement between these two distributions in the range 5 GeV $\leq E_T \leq$ 8 GeV.

The numerical results of this background study are shown in table 7.1. As already stated, the $E_T$bin width was chosen as small as possible with the

$E_{T,had}$ (GeV)	5–7.5	7.5–10	10–12.5
number of DIS jets which look like a photon	12.9	21.2	6.3
95% confidence level upper limit	20.6	30.5	12.2
number of DIS jets	18932	13524	6988
photon/jet x 10^{-3}	0.862	1.52	0.971
photon/jet x 10^{-3} (95% C.L.)	1.34	2.21	1.80
number of photoproduction jets	19187	17695	8559
number of background events	16.5	26.9	8.3
number of background events (95% C.L.)	25.7	39.1	15.4

Table 7.1: Numerical results of prompt photon background study.

available statistics. The second row of the table is the numerator of the 'photon/jet' fraction, the number of events in which the jet is misidentified as a single photon, while the third row is the 95% confidence level upper limit based on this number. Non-integer values occur because of the statistical subtraction of inelastic Compton events. Dividing these numbers by the fourth row of the table, the denominator of the 'photon/jet' fraction, yields (aside from a correction due to different E_T shapes) the 'photon/jet' fraction and its 95% confidence level upper limit. Multiplying these by the number of photoproduction jets gives the number of background events in each bin and the corresponding 95% confidence level upper limit. These three bins must be added together to give a final result. This study predicts a background of 52 events (with an upper limit of 80 events) in the prompt photon analysis due to jets being misidentified as single photons. Table 7.2 shows that the results don't change dramatically when each of the main cuts is varied by a reasonable amount.

The actual background calculated in the prompt photon analysis is 36 $\pm$

cut variation	nominal	95% C.L.
standard cuts	52	80
no E_T shape correction	49	76
$40 \leq \theta_{had} \leq 126 \rightarrow 44 \leq \theta_{had} \leq 122$	46	74
Ehadfrac $\geq 0.5 \rightarrow$ Ehadfrac ≥ 0.6	55	87
Ehadfrac $\geq 0.5 \rightarrow$ Ehadfrac ≥ 0.4	43	67
decrease by 50% number of Comptons subtracted	53	81
increase by 50% number of Comptons subtracted	44	70
change E_T^{jet}(cal $\rightarrow$ hadron level) from 14% to 17%	49	77
change E_T^{jet}(cal $\rightarrow$ hadron level) from 14% to 11%	48	74
5 GeV $\leq E_T^{jet} \leq$ 11 GeV $\rightarrow$ 5 GeV $\leq E_T^{jet} \leq$ 10 GeV	46	71

Table 7.2: Sensitivity of background estimation to variations of the cuts.

14 events for $X_\gamma \geq 0.8$. This is the sum of events in figure nn.n(X_γ background plot not made yet) above 0.8 ($\sim$31 events) and those events in figure nn.m(X_γ signal plot not made yet) due to quark radiation according to Pythia Monte Carlo ($\sim$5 events). The quark radiation events are included in this 'background' because they are present in the DIS sample as well. The total signal plus background with $X_\gamma \geq 0.8$ is 90 events.

The 52 events (with an upper limit of 80 events) obtained from this independent background study using DIS events is consistent with the 36 $\pm$ 14 events determined in the prompt photon analysis itself.

Chapter 8

Conclusions

- quick summary
- (future?: more lumi, inclusive measurement)

Appendix A

Title of Appendix A

Reserved for future use.

Appendix B

Title of Appendix B

Reserved for future use.

References

1. L. E. Gordon and W. Vogelsang, Phys. Rev. **D50**, 1901 (1994).

2. L. E. Gordon and W. Vogelsang, Phys. Rev. **D52**, 58 (1995).

3. A. C. Bawa and W. J. Stirling, J. Phys. **G14**, 1353 (1988).

4. A. C. Bawa, M. Krawczyk and W. J. Stirling, Z. Phys. **C50**, 293 (1991).

5. ZEUS Collab., The ZEUS Detector, Status Report, DESY 1993.

6. T. Sjöstrand, Computer Physics Commun. 82 (1994) 74.

7. H. U. Bengtsson and T. Sjöstrand, Comp. Phys. Comm. **C46**, 43 (1987).

8. B. Anderson, G. Gustafson, G. Ingelmann, T. Sjöstrand, Phys. REv. 97 (1983) 31.

9. R. Brinkman, 'HERA'. DESY-HERA 88-03 (1988)

10. H. Abromowicz, A. Caldwell and R. Sinkus, Nucl. Inst. Meth. A365 (1995) 508.

11. ZEUS SRTD Group, DESY 97-157 (1997).

12. R. S. Gilmore, *Single particle detection and measurement*, Taylor and Francis (1987).

13. W. R. Leo, W.R., *Techniques for Nuclear and Particle Physics Experiments*, Springer-Verlag, (1987).

14. A. Andresen, Nucl. Inst. Meth. A309 (1991) 101.

15. W.H. Smith et al., Nucl. Instr. Meth. A355 (1995) 278-294.

16. DJANGO 6.24, K. Charchula, G.A. Schuler and H. Spiesberger, Comp. Phys. Comm. 81 (1994) 381.

17. HERACLES 4.5.2, A. Kwiatkowski, H.–J. Möhring and H. Spiesberger, Comp. Phys. Comm. 69 (1992) 155.

18. B. Andersson et al., Z. Phys. C 43 (1989) 625.

19. ARIADNE 4.08, L. Lönnblad, Comp. Phys. Comm. 71 (1992) 15; L. Lönnblad, Z. Phys. C 65 (1995) 285.

20. LEPTO 6.5, G. Ingelman, A. Edin and J. Rathsman, Comp. Phys. Comm. 101 (1997) 108.

21. D. Bandyopadhyay, ZEUS-Note 93-013 (1993).